Current effects on scattering of surface gravity waves by bottom topography

Rudy Magne, Fabrice Ardhuin

Current effects on scattering of surface gravity waves by bottom topography

By RUDY MAGNE[1,2] AND FABRICE ARDHUIN[1]

[1]Centre Militaire d'Océanographie, Service Hydrographique et Océanographique de la Marine, 29275 Brest, France

[2]Laboratoire de Sondages Electromagnétique de l'Environnement Terrestre, Université de Toulon et du Var, La Garde, France

ardhuin@shom.fr

(Received 8 September 2005 (draft))

Scattering of random surface gravity waves by small amplitude topography in the presence of a uniform current is investigated theoretically. This problem is relevant to ocean waves propagation on shallow continental shelves where tidal currents are often significant. A perturbation expansion of the wave action to second order in powers of the bottom amplitude yields an evolution equation for the wave action spectrum. Based on numerical calculations for sinusoidal bars, a mixed surface-bottom bispectrum that arises in the lowest order evolution equation is unlikely to be significant in most oceanic conditions. Neglecting that term, the present theory yields a closed wave equation with a scattering source term that gives the rate of exchange of the wave action spectrum between wave components, with conservation of the total action at each absolute frequency. With and without current, the scattering term yields reflection coefficients for the amplitudes of waves that converge, in the limit of small bottom amplitudes and small Froude numbers, to the results of previous theories for monochromatic waves propagating in one dimension over sinusoidal bars. In particular, the frequency of the waves that experience the maximum reflection is shifted by the current, as the surface wavenumber k changes for a fixed absolute frequency. Over sandy continental shelves, tidal currents are known to generate sandwaves with scales comparable to those of surface waves and elevation spectra that roll-off sharply at high wavenumbers. Application of the theory to such a real topography suggests that scattering mainly results in a broadening of the directional wave spectrum, due to forward scattering, while the back-scattering is generally weaker. The current may strongly influence surface gravity wave scattering by selecting different bottom scales with widely different spectral densities due the sharp bottom spectrum roll-off.

1. Introduction

Following the early observations of Heathershaw (1982), a considerable body of knowledge has been accumulated on the scattering of small amplitude surface gravity waves by periodic bottom topography. An asymptotic theory for small bottom amplitudes, that reproduces the observed scattering of monochromatic waves over a few sinusoidal bars, was put forward by Mei (1985), leading to practical phase-resolving equations that may be used to model this phenomenon for more general bottom shapes (Kirby 1986). For sinusoidal bottoms of wavenumber l, Mei (1985) proposed an approximate analytical solution. In two dimensions (one horizontal and the vertical) this solution yields simple

expressions for the wave amplitude reflection coefficient R, as a function of the mismatch between the wavenumber of the surface waves k and the resonant value $l/2$, for which R is maximum due to Bragg resonance. Beyond a cut-off value of that mismatch, it was found that the incident and reflected wave amplitudes oscillate in space instead of decreasing monotonically from the incident region. In three dimensions the Bragg resonance condition becomes $\boldsymbol{k} = \boldsymbol{l} + \boldsymbol{k}'$ and $k = k'$, with k, k', and l the norms of the horizontal wave-vectors $\boldsymbol{k}$, $\boldsymbol{k}'$, and $\boldsymbol{l}$. A uniform current was later introduced by Kirby (1988). The resonant condition is modified in that case, with $k \neq k'$ if incident and reflected waves propagate at different angles relative to the current direction. Other contributions have shown that higher-order theories are necessary to represent the sub-harmonic resonance observed over a bottom that is a superposition of two components of different wavelengths (Guazzelli, Rey & Belzons 1992). Such sub-harmonic resonance was found to have as large an effect as the lowest order resonance for bottom amplitudes of only 25% of the water depth, due to a general stronger reflection for relatively longer waves. However, these methods are still prohibitively expensive for investigating the propagation of random waves over distances larger than about 100 wavelengths, and the details of the bottom are typically not available over large areas. Besides, a consistent phase-averaged wave energy evolution equation is also necessary for the investigation of the long waves associated with short wave groups (Hara & Mei 1987).

The large scale behaviour of the wave field may rather be represented by the evolution of the wave action spectrum assuming random phases. Such an approach was already proposed by Hasselmann (1966) for wind-wave propagation, and Elter & Molyneux (1972) for the calculation of tsunami propagation. A proper theory for the evolution of the wave spectrum can be obtained from a solvability condition, a method similar to that of Mei (1985) and Kirby (1988), but applied to the action spectral densities instead of the amplitudes of monochromatic waves. In the absence of currents the correct form of that equation was first obtained by Ardhuin & Herbers (2002, hereinafter referred to as AH) using a two scale approach. They decomposed the water depth $H - h$ in a slowly varying depth H, that causes shoaling and refraction, and a rapidly varying perturbation h with zero mean, that causes scattering. The resulting scattering was shown to be consistent with the dramatic increase of the directional width of the wave spectra observed on the North Carolina continental shelf. (Ardhuin *et al.* 2003a, 2003b). Recently, Magne *et al.* (2005, hereinafter referred to as MAHR) showed that AH's theory gives the same damping of incident waves as a Green function solution applied to any two dimensional topography (random or not) of small amplitude (see also Pihl, Mei & Hancock 2002; Mei & Hancock 2003). Investigating the applicability limits of the scattering term of AH, MAHR also performed numerical calculations, comparing AH's theory to the accurate matched-boundary model of Rey (1995) that uses a decomposition of the bottom in a series of steps, including evanescent modes. The numerical results show that AH's theory is generally limited by the relative bottom amplitude $\eta = \max(h)/H$ rather than the bottom slope.

The resulting expression of the scattered energy as a Bragg scattering term is consistent with results for scattering of acoustic and electromagnetic waves obtained by the small perturbation method, valid in the limit of small $k \max(h)$ with k the wavenumber of the propagating waves (Rayleigh 1896, see Elfouhaily & Guerin 2004 for a review of this and other approximations). Since there is no scattering for $kH >> 1$, as the waves do not 'feel' the bottom, the small parameter $\eta = \max(h)/H$ may be used in our context, instead of the more general $k \max(h)$. The scattering strength is thus entirely determined by the bottom elevation variance spectrum at the bottom scales resonant with the incident waves. Based on these results, Mei's (1985) theory should yield the same reflection

coefficient as AH's theory in the limit of small bottom amplitudes. Yet, AH predict that the wave amplitude in 2D would decay monotonically, which is not compatible with the oscillatory nature of Mei's theory for large detunings from resonance. Further, outside of the surf zone and the associated multiple bar systems, the application of AH's theory is most relevant in areas where the bottom topography changes significantly on the scale of the wavelengths of swells. This often corresponds, over sand, to the presence of sandwaves. These sandwaves are generated by currents, and particularly by tidal currents (e.g. Dalrymple Knoght & Lambiase 1978; Idier, Erhold & Garlan 2002). It is thus logical to seek a theory for the scattering of waves in the presence of currents. A first theory was proposed by Kirby (1988), in the form of an extension of Mei (1985), with waves in a uniform current over a sinusoidal bottom.

The present paper provides an extension of AH's theory for the case of uniform currents in § 2, and a detailed discussion of the differences between this theory and those of Mei (1985) and Kirby (1988) in § 3. Finally the oceanographic effects of the current are investigated in § 4 using a spectral phase-averaged numerical model, predicting the evolution of the wave action spectrum, and detailed measurements of the topography in the southern North Sea. Conclusions follow in § 5. Further details on the source term derivation, and model results may be found in Magne (2005).

2. Theory

2.1. *General formulation*

The variation in the action spectral density due to wave-bottom scattering is derived following the method of AH, now including the effect of a uniform current. We consider weakly nonlinear random waves propagating over an irregular bottom with a constant mean depth H and random small-scale topography $h(\boldsymbol{x})$, with $\boldsymbol{x}$ the horizontal position vector, so that the bottom elevation is given by $z = -H + h(\boldsymbol{x})$ where z is the elevation relative to the mean water level. The free surface is at $z = \zeta(\boldsymbol{x}, t)$. Extension to current and mean depth variations on a large scale is expected to follow from a two-scale approximation, similar to the effect of large scale depth variation (AH). When the depth varies in the flow direction, the current should also vary so that the flows remains non-divergent. Perturbations of the current should thus be of the order of ηU with $\eta = \max\{h/H\}$, and may scatter waves (Bal & Chou 2002). As far as this and other effects do not modify the wave-bottom resonance, they should only contribute separate source terms, and shoaling and refraction terms. Further, for a depth-varying current, U should be regarded as the wave advection velocity (Andrews & McIntyre 1978, see Kirby & Chen 1989 for practical approximate expressions).

The maximum surface slope is caracterized by ε and we shall assume that $\varepsilon^3 \ll \eta^2$ so that the bottom scattering contributions to the wave energy to order η^2 are much larger than the resonant non-linear four wave interactions (Hasselmann 1962) and may be neglected. For shallow water waves ($kH << 1$) a stricter inequality is needed to prevent triad wave-wave interactions to enter the energy evolution equation at the same order as bottom scattering.

The solution is obtained in a frame of reference moving with the current, so that the current only introduces a modification of the bottom boundary condition. The governing wave equations are thus given by Laplace's equation for the wave potential, the bottom kinematic boundary conditions and a combination of Bernouilli's equation with the free

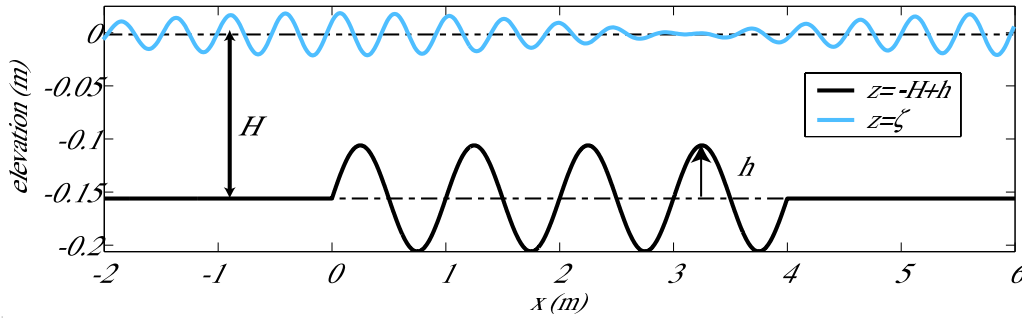

FIGURE 1. Definition sketch of the mean water depth H, and relative bottom elevation h, in the particular case of the sinusoidal bottom used in § 3.

surface kinematic boundary condition,

$$\boldsymbol{\nabla}^2\Phi + \frac{\partial^2\Phi}{\partial z^2} = 0 \quad \text{for} \quad -H + h \leqslant z \leqslant \zeta, \tag{2.1}$$

$$\frac{\partial\Phi}{\partial z} = \frac{\partial h}{\partial t} + \boldsymbol{\nabla}\Phi\cdot\boldsymbol{\nabla}h \quad \text{at} \quad z = -H + h, \tag{2.2}$$

$$\frac{\partial^2\phi}{\partial t^2} + g\frac{\partial\phi}{\partial z} = g\boldsymbol{\nabla}\phi\cdot\boldsymbol{\nabla}\zeta - \boldsymbol{\nabla}\phi\cdot\frac{\partial\boldsymbol{\nabla}\phi}{\partial t} - \frac{\partial\phi}{\partial z}\frac{\partial^2\phi}{\partial t\partial z} \quad \text{at} \quad z = \zeta. \tag{2.3}$$

The symbol $\boldsymbol{\nabla}$ represents the usual gradient operator restricted to the two horizontal dimensions.

Following Hasselmann (1962) we shall approximate h and ϕ with discrete sums, and take the limit to continuous integrals after deriving expressions for the evolution of the phase-averaged wave energy. The current $\boldsymbol{U}$ introduced a transformation of the horizontal coordinates $\boldsymbol{x}' = \boldsymbol{x} + \boldsymbol{U}t$, where $\boldsymbol{x}$ and $\boldsymbol{x}'$ are the coordinates in the moving and fixed frames, respectively. The bottom elevation thus becomes

$$h(\boldsymbol{x}) = \sum_{\boldsymbol{l}} G_{\boldsymbol{l}}\mathrm{e}^{\mathrm{i}\boldsymbol{l}\cdot[\boldsymbol{x}+\boldsymbol{U}t]}. \tag{2.4}$$

We look for a velocity potential solution in the form

$$\phi(\boldsymbol{x}, z, t) = \sum_{\boldsymbol{k},s} \Phi^s_{\boldsymbol{k}}(z, \alpha t)\mathrm{e}^{\mathrm{i}[\boldsymbol{k}\cdot\boldsymbol{x} - s\sigma t]}, \tag{2.5}$$

where σ and ω are the radian frequencies in the moving and fixed frame, respectively. $\boldsymbol{l}$ and $\boldsymbol{k}$ are the bottom and surface wavenumber, respectively, s is a sign index equal to 1 or -1, and $s\sigma = s\omega - \boldsymbol{k}\cdot\boldsymbol{U}$. In the moving frame of reference, components with $s = 1$ propagate in the direction of the vector $\boldsymbol{k}$, while components with $s = -1$ propagate in the opposite direction. The amplitudes $\Phi^s_{\boldsymbol{k}}$ are slowly modulated in time, with a slowness defined by the small parameter α. Because ϕ is a real quantity we also have $\overline{\Phi^s_{\boldsymbol{k}}} = \Phi^{-s}_{-\boldsymbol{k}}$.

Numerical calculations by MAHR showed that the reflection coefficient predicted by AH were accurate for any bottom slope, but appeared to be limited by the relative bottom amplitude $\eta = h/H$. We thus chose to expand the bottom boundary condition and wave potential in powers of η,

$$\phi = \phi_0 + \eta\phi_1 + \eta^2\phi_2 + \cdots \tag{2.6}$$

The boundary conditions (2.3) and (2.2) are expressed at $z = 0$ and $z = -H$, respectively, using Taylor series of ϕ about $z = -H$ and $z = 0$.

The spectral statistics of free wave components can be expressed in terms of covariances

$F^{\Phi}_{i,j,k}$ of the velocity potential amplitudes,

$$F^{\Phi}_{i,j,k} = \langle \Phi^{+}_{i,\boldsymbol{k}} \Phi^{-}_{j,-\boldsymbol{k}} + \Phi^{-}_{i,-\boldsymbol{k}} \Phi^{+}_{j,\boldsymbol{k}} \rangle. \tag{2.7}$$

The contribution of the complex conjugate pairs of components $(\boldsymbol{k}, +)$ and $(-\boldsymbol{k}, -)$ are combined in (2.7) so that $F^{\Phi}_{i,j,k}$ is the covariance of all waves with wavenumber magnitude k propagating in the direction of $\boldsymbol{k}$. In the limit of small wavenumber separation, a continuous slowly-varying cross-spectrum can be defined (e.g. Priestley 1981, ch.11; see also AH),

$$F^{\Phi}_{i,j}(\boldsymbol{k}) = \lim_{|\Delta k| \to 0} \frac{F^{\Phi}_{i,j,k}}{\Delta k_x \Delta k_y}. \tag{2.8}$$

The definition of all spectral densities are chosen so that the integral over the entire wavenumber plane yields the total covariance of ϕ_i and ϕ_j. The bottom elevation spectrum in discrete form is given by $F^{G}_{\boldsymbol{l}} = \langle G_{\boldsymbol{l}} G_{-\boldsymbol{l}} \rangle$ and in continuous form by

$$F^{B}(\boldsymbol{l}) = \lim_{|\Delta l| \to 0} \frac{F^{G}_{\boldsymbol{l}}}{\Delta l_x \Delta l_y}, \tag{2.9}$$

and verifies,

$$\int_{-\infty}^{\infty} \int_{-\infty}^{\infty} F^{B}(\boldsymbol{l}) \mathrm{d}l_x \mathrm{d}l_y = \lim_{L \to \infty} \frac{1}{L^2} \int_{-L/2}^{L/2} \int_{-L/2}^{L/2} h^2(x, y) \mathrm{d}x \mathrm{d}y \tag{2.10}$$

$N_{i,j}(\boldsymbol{k})$ is defined as the $(i+j)^{\text{th}}$ order depth-integrated wave action contribution from correlation between i^{th} and j^{th} order components with wavenumber k. For freely propagating waves, and following the common usage in non-accelerated reference frames, the gravity g is left out, so that the action has units of meters squared times second. Accurate to second order in ε and η (Andrews & McIntyre 1978), $N_{i,j}$ is given from the velocity potential by the linear relation,

$$N_{i,j}(\boldsymbol{k}) = \frac{k}{g\sigma} F^{\Phi}_{i,j}(\boldsymbol{k}) \tanh(kH). \tag{2.11}$$

The spectral wave action is thus,

$$N(\boldsymbol{k}) = \sum_i N_i(\boldsymbol{k}) = \sum_i \sum_j N_{i,i-j}(\boldsymbol{k}). \tag{2.12}$$

We shall now solve for the velocity potential in the frame of reference moving with the current.

2.2. *Zeroth-order solution*

In the moving frame of reference, the governing equations for ϕ_0 are unchanged from the case with a current. The solution is thus

$$\phi_0 = \sum_{\boldsymbol{k}, s} \frac{\cosh(k(z+H))}{\cosh(kH)} \Phi^{s}_{0,\boldsymbol{k}} \mathrm{e}^{\mathrm{i}[\boldsymbol{k}\cdot\boldsymbol{x} - s\sigma t]}, \tag{2.13}$$

where intrinsic frequency σ is the positive root of the linear dispersion relation,

$$\sigma^2 = gk \tanh(kH). \tag{2.14}$$

2.3. *First-order solution*

The equations at order η are

$$\boldsymbol{\nabla}^2\phi_1 + \frac{\partial^2\phi_1}{\partial z^2} = 0 \quad \text{for} \quad -H \leqslant z \leqslant 0, \tag{2.15}$$

$$\frac{\partial\phi_1}{\partial z} = -h\frac{\partial^2\phi_0}{\partial z^2} + \frac{\partial h}{\partial t} + \boldsymbol{\nabla}\phi_0 \cdot \boldsymbol{\nabla} h \qquad \text{at} \qquad z = -H, \tag{2.16}$$

and

$$\frac{\partial^2\phi_1}{\partial t^2} + g\frac{\partial\phi_1}{\partial z} = NL_1 \qquad \text{at} \qquad z = 0, \tag{2.17}$$

where the non-linear terms NL_1 force a bound wave solution ϕ_1^{nl} (Hasselmann 1962) that will be neglected here because it does not modify our second order wave energy balance. The small-scale variation h that causes scattering now appears in the bottom boundary condition. A general solution for the (unchanged) Laplace equation (2.15) is given by the following superposition of free and bound wave components, with amplitudes $\Phi^{s_3}_{2,\boldsymbol{k}}$ and $\Phi^{si,s_3}_{1,\boldsymbol{k}}$ respectively,

$$\phi_1 = \sum_{\boldsymbol{k},s_3=-1,0,1}\left[\frac{\cosh\left[k(z+H)\right]}{\cosh(kH)}\Phi^{s_3}_{1,\boldsymbol{k}}(t) + \frac{\sinh\left[k(z+H)\right]}{\cosh(kH)}\Phi^{si,s_3}_{1,\boldsymbol{k}}(t)\right]\mathrm{e}^{\mathrm{i}\boldsymbol{k}\cdot\boldsymbol{x}} \tag{2.18}$$

Substitution of (2.18) in the bottom boundary condition (2.16) yields

$$\frac{k}{\cosh(kH)}\Phi^{si,s}_{1,\boldsymbol{k}}(t) = -\sum_{\boldsymbol{k'}}\frac{\boldsymbol{k'}\cdot\boldsymbol{k}}{\cosh(k'H)}\Phi^{s}_{1,\boldsymbol{k'}}G_{\boldsymbol{k}-\boldsymbol{k'}}\mathrm{e}^{\mathrm{i}\left[(\boldsymbol{k}-\boldsymbol{k'})\cdot\boldsymbol{U}-s\sigma'\right]t}, \tag{2.19}$$

for $s = \pm 1$. The amplitude of the $s_3 = 0$ term forced by the $\partial h/\partial t$ term in (2.16) is given by

$$\Phi^{si,0}_{1,\boldsymbol{k}}(t) = i\boldsymbol{k}\cdot\boldsymbol{U}\frac{\cosh(kH)}{k}G_{\boldsymbol{k}}\mathrm{e}^{\mathrm{i}\boldsymbol{k}\cdot\boldsymbol{U}t}. \tag{2.20}$$

Replacing now (2.18) in the surface boundary condition (2.17), yields an equation for $\Phi^{s_3}_{1,\boldsymbol{k}}$,

$$\left(\frac{d^2}{dt^2} + \sigma^2\right)\Phi^{s}_{1,\boldsymbol{k}}(t) = \sum_{\boldsymbol{k'}}M^s(\boldsymbol{k},\boldsymbol{k'})\Phi_{1,\boldsymbol{k'}}G_{\boldsymbol{k}-\boldsymbol{k'}}\mathrm{e}^{\mathrm{i}\left[(\boldsymbol{k}-\boldsymbol{k'})\cdot\boldsymbol{U}-s\sigma'\right]t}, \tag{2.21}$$

for $s = \pm 1$, with

$$M^s(\boldsymbol{k},\boldsymbol{k'}) = \left\{gk - \left[(\boldsymbol{k}-\boldsymbol{k'})\cdot\boldsymbol{U} - s\sigma'\right]^2\tanh(kH)\right\}\frac{\boldsymbol{k'}\cdot\boldsymbol{k}}{k}\frac{\cosh(kH)}{\cosh(k'H)}. \tag{2.22}$$

For the $s_3 = 0$ component we have,

$$\left(\frac{d^2}{dt^2} + \sigma^2\right)\Phi^{0}_{1,\boldsymbol{k}}(t) = C(\boldsymbol{k})G_{\boldsymbol{k}}\mathrm{e}^{\mathrm{i}\boldsymbol{k}\cdot\boldsymbol{U}t} \tag{2.23}$$

with

$$C(\boldsymbol{k}) = \mathrm{i}\boldsymbol{k}\cdot\boldsymbol{U}\left[\frac{(\boldsymbol{k}\cdot\boldsymbol{U})^2}{k}\sinh(kH) - g\cosh(kH)\right]. \tag{2.24}$$

The forced harmonic oscillator equation (2.21) leads to

$$\Phi^{s}_{1,\boldsymbol{k}}(t) = \sum_{\boldsymbol{k'}}M^s(\boldsymbol{k},\boldsymbol{k'})\Phi^{s}_{0,\boldsymbol{k'}}G_{\boldsymbol{k}-\boldsymbol{k'}}f_1(\sigma,\boldsymbol{l}\cdot\boldsymbol{U} - s\sigma'), \tag{2.25}$$

with the function f_1 defined in Appendix A, and

$$\Phi^0_{1,\boldsymbol{k}}(t) = C(\boldsymbol{k}) G_{\boldsymbol{k}} f_1(\sigma, \boldsymbol{k}\cdot\boldsymbol{U}). \tag{2.26}$$

The components of amplitude $\Phi^0_{1,\boldsymbol{k}}$ and $\Phi^{si,0}_{1,\boldsymbol{k}}$ correspond to stationary waves such as generated by the bottom topography in rivers (e.g. Fredsøe, 1974). These components do not give rise to resonant interaction except at the critical Froude number, when the current is equal to the phase speed of the waves. This solution is identical to equation (2.9) in Kirby (1988) for monochromatic waves. The second term gives rise to scattered waves and reduces to the form given by AH when U goes to zero.

2.3.1. *First order energy*

The lowest order perturbation of the wave energy by scattering involves ϕ_1, and because it is a quadratic term, it is found in the first order covariance

$$F^{\Phi}_{1,0,\boldsymbol{k}} + F^{\Phi}_{0,1,\boldsymbol{k}} = 4\mathrm{Re}\left(\langle \Phi^+_{0,\boldsymbol{k}} \Phi^-_{1,-\boldsymbol{k}} \rangle\right), \tag{2.27}$$

with Re denoting the real part. Including only the non-bounded terms, we get

$$F^{\Phi}_{1,0,\boldsymbol{k}} + F^{\Phi}_{0,1,\boldsymbol{k}} = 4\mathrm{Re}\left[\sum_{\boldsymbol{k'}} M^+(\boldsymbol{k},\boldsymbol{k'}) \langle \Phi^+_{0,\boldsymbol{k'}} \Phi^-_{0,-\boldsymbol{k}} G_{\boldsymbol{k}-\boldsymbol{k'}} \rangle f_1(\sigma, \boldsymbol{l}\cdot\boldsymbol{U} - \sigma') \mathrm{e}^{\mathrm{i}\sigma t}\right]. \tag{2.28}$$

Although this term was assumed to be zero in AH, it is not zero for sinusoidal bottoms with partially standing waves, and may become significant at resonance due to the function f_1. At this order, another term is needed to balance this energy transfer. In uniform conditions, the time evolution of the wave field requires that the non-stationarity must come into play so that $\alpha \approx \eta$, the non-stationary term is given by AH (their appendix D),

$$\frac{\partial \left[N^{\mathrm{ns}}_{1,0}(\boldsymbol{k}) + N^{\mathrm{ns}}_{0,1}(\boldsymbol{k})\right]}{\partial t} = -\frac{\partial N_0(\boldsymbol{k})}{\partial t}. \tag{2.29}$$

In order to simplify the discussion, we shall briefly assume that there is no current and that the waves are unidirectional. In that case, $\boldsymbol{k'} = -\boldsymbol{k}$ and $M(\boldsymbol{k},\boldsymbol{k'}) = gk^2/\cosh^2(kH)$. Replacing (2.28) in (2.11) and combining it with (2.29) yields the action balance

$$\frac{\partial N_{0,\boldsymbol{k}}}{\partial t} = \frac{\partial}{\partial t}\left[\frac{k}{\sigma}\tanh(kH)\left(F^{\Phi}_{1,0,\boldsymbol{k}} + F^{\Phi}_{0,1,\boldsymbol{k}}\right)\right] = \mathrm{Im}\left(\frac{4k\sigma^2}{g^2\sinh(2kH)}\langle \Phi^+_{0,\boldsymbol{k}} \Phi^-_{0,\boldsymbol{k}} G_{-2k}\rangle\right), \tag{2.30}$$

with Im denoting the imaginary part.

For a real bottom (e.g. random or consisting of a finite series of sinusoidal bars), the evaluation of (2.28) is not simple. Indeed, for directionally spread random waves and with a current, using $N(\boldsymbol{k}) = N_0(\boldsymbol{k})\left[1 + O(\eta)\right]$ and taking the limit to continuous surface and bottom spectra yields

$$\frac{\partial N(\boldsymbol{k})}{\partial t} = S_1(\boldsymbol{k}) = \int_{-\infty}^{\infty}\int_{-\infty}^{\infty} \frac{4\boldsymbol{k}\cdot\boldsymbol{k'}}{2g\cosh(kH)\cosh(k'H)} \mathrm{Im}\left[Z(\boldsymbol{k},\boldsymbol{k'})\right] \mathrm{d}k'_x \mathrm{d}k'_y, \tag{2.31}$$

with the mixed surface bottom bispectrum Z defined by

$$Z(\boldsymbol{k},\boldsymbol{k'}) = \lim_{\Delta\boldsymbol{k}\to\infty} \langle \frac{\Phi^+_{1,\boldsymbol{k}} \Phi^-_{1,-\boldsymbol{k'}} G_{-k-k'}}{\left(\Delta\boldsymbol{k}\right)^2} \rangle, \tag{2.32}$$

with $\boldsymbol{k} = k(\cos\theta, \sin\theta)$ and $\boldsymbol{k'} = k(\cos\theta', \sin\theta')$. Z is identical to a classical bispectrum (e.g. Herbers *et al.* 2003) with one surface wave amplitude replaced by a bottom amplitude, and a similar expression is fond for a non-zero current. Since we have neglected

non-linear effects, only the waves that have the same absolute frequency interact. Thus the phase coupling of all other wave component pairs is random, and the bispectrum is zero for $\sigma' \neq \sigma + \boldsymbol{l}\cdot\boldsymbol{U}$. The energy balance (2.31) is not closed, and requires a knowledge of the wave phases that are not available in a phase-averaged model. This contribution of the mixed bispectrum will thus be evaluated below, in order to investigate in which cases it may be neglected or parameterized. It is expected that S_1 is generally negligible because MAHR have neglected S_1, and still found a good agreement of the second order energy balance, with an exact numerical solution.

2.3.2. *Second order energy*

At the next order, one of the contributions from the covariance of the velocity potential amplitudes is given by

$$F^{\Phi}_{1,1,\boldsymbol{k}} = 2\langle \Phi^{+}_{1,\boldsymbol{k}} \Phi^{-}_{1,-\boldsymbol{k}} \rangle. \tag{2.33}$$

Using (2.25), (2.33) can be re-written as

$$\frac{F^{\Phi}_{1,1,\boldsymbol{k}}}{\Delta\boldsymbol{k}} = 2\sum_{\boldsymbol{k'}} \left|M^{+}(\boldsymbol{k},\boldsymbol{k'})\right|^2 \frac{\left\langle \left|\Phi^{+}_{0,\boldsymbol{k'}}\right|^2 \right\rangle}{\Delta\boldsymbol{k'}} \frac{\left\langle \left|G_{\boldsymbol{k}-\boldsymbol{k'}} G_{-\boldsymbol{k}+\boldsymbol{k'}}\right|^2 \right\rangle}{\Delta\boldsymbol{k}} \left|f_1(\sigma, \boldsymbol{l}\cdot\boldsymbol{U}-\sigma')\right|^2 \Delta\boldsymbol{k'}, \tag{2.34}$$

in which

$$\langle f_1(\sigma, \boldsymbol{l}\cdot\boldsymbol{U}-\sigma') f_1(\sigma, -\boldsymbol{l}\cdot\boldsymbol{U}+\sigma')\rangle = \frac{\pi t}{2\sigma^2}\delta\left[\sigma' - (\sigma + \boldsymbol{l}\cdot\boldsymbol{U})\right] + O(1). \tag{2.35}$$

δ is the one-dimension Dirac distribution, infinite where the argument is zero. Taking the limit of (2.34) when $\Delta\boldsymbol{k} \to 0$, and changing variables from (k'_x, k'_y) to (σ', θ') yields

$$F^{\Phi}_{1,1}(t,\boldsymbol{k}) = \frac{\pi t}{2\sigma^2}\int_{\theta'}\int_{\sigma'} \left|M^{+}(\boldsymbol{k},\boldsymbol{k'})\right|^2 F^{\Phi}_{1,1}(\boldsymbol{k'}) F^{B}(\boldsymbol{k}-\boldsymbol{k'}) \frac{k'}{C'_g}\delta\left[\sigma' - (\sigma + \boldsymbol{l}\cdot\boldsymbol{U})\right] d\sigma' \mathrm{d}\theta' + O(1). \tag{2.36}$$

Only the terms for which $\sigma' = \sigma + \boldsymbol{l}\cdot\boldsymbol{U}$ contribute to the integral. Thus $M^s(\boldsymbol{k},\boldsymbol{k'}) = M(\boldsymbol{k},\boldsymbol{k'})$, with

$$\begin{aligned} M(\boldsymbol{k},\boldsymbol{k'}) &= \left[gk - \sigma^2\tanh(kH)\right]\frac{\boldsymbol{k'}\cdot\boldsymbol{k}}{k}\frac{\cosh(kH)}{\cosh(k'H)}, \\ &= \frac{g\boldsymbol{k}\cdot\boldsymbol{k'}}{\cosh(kH)\cosh(k'H)}. \end{aligned} \tag{2.37}$$

Using the relation between velocity potential and action given by (2.11), and evaluating the integral over σ', one obtains

$$N_{1,1}(t,\boldsymbol{k}) = \frac{\pi t}{2}\int_{\theta'} M^2(\boldsymbol{k},\boldsymbol{k'})\frac{N_{0,0}(\boldsymbol{k'})}{\sigma\sigma'}F^{B}(\boldsymbol{k}-\boldsymbol{k'})\frac{k'}{C'_g}d\theta' + O(1). \tag{2.38}$$

2.4. *Second order solution*

Because we have computed one second order energy term, we now have to compute all other second order terms in (2.12) to obtain the solvability condition. This requires solving for the second order potential ϕ_2, that is a solution of

$$\boldsymbol{\nabla}^2\phi_2 + \frac{\partial^2\phi_2}{\partial z^2} = 0 \qquad \text{for} \qquad -H \leqslant z \leqslant 0, \tag{2.39}$$

$$\frac{\partial\phi_2}{\partial z} = -h\frac{\partial^2\phi_1}{\partial z^2} - \frac{h^2}{2}\frac{\partial^3\phi_0}{\partial z^3} + \boldsymbol{\nabla}\phi_1\cdot\boldsymbol{\nabla}h + \boldsymbol{\nabla}(h\frac{\partial\phi_0}{\partial z})\cdot\boldsymbol{\nabla}h \qquad \text{at} \qquad z = -H, \tag{2.40}$$

that simplifies because odd vertical derivatives of ϕ_0 are zero at $z=-H$,

$$\frac{\partial\phi_2}{\partial z} = -h\frac{\partial^2\phi_1}{\partial z^2} + \boldsymbol{\nabla}\phi_1\cdot\boldsymbol{\nabla}h \qquad \text{at} \qquad z=-H, \tag{2.41}$$

and

$$\frac{\partial^2\phi_2}{\partial t^2} + g\frac{\partial\phi_2}{\partial z} = \mathrm{i}\sum_{\boldsymbol{k},s} 2s\sigma\frac{\partial\Phi^s_{0,\boldsymbol{k}}}{\partial t}\mathrm{e}^{\mathrm{i}(\boldsymbol{k}\cdot\boldsymbol{x}-s\omega t)} + NL_2 \qquad \text{at} \qquad z=0. \tag{2.42}$$

Ignoring the non-linear contributions NL_2, the solution ϕ_2 is given by the following form,

$$\phi_2 = \phi_2^{\mathrm{ns}} + \sum_{\boldsymbol{k},s_3=-1,0,1}\left[\frac{\cosh(k(z+H))}{\cosh(kH)}\Phi^{s_3}_{2,\boldsymbol{k}}(t) + \frac{\sinh(k(z+H))}{\cosh(kH)}\Phi^{si,s_3}_{2,\boldsymbol{k}}(t)\right]\mathrm{e}^{\mathrm{i}\boldsymbol{k}\cdot\boldsymbol{x}}. \tag{2.43}$$

The non-stationarity term ϕ_2^{ns} is defined as the solution of the second order equations forced by only the first term on the right-hand side of (2.41) and is given by AH. Following the method used at first order, substitution of (2.43) in the bottom boundary condition (2.41) leads to, for $s=\pm1$,

$$\Phi^{si,s}_{2,\boldsymbol{k}}(t) = -\sum_{\boldsymbol{k}'}\frac{\boldsymbol{k}'\cdot\boldsymbol{k}}{k}\frac{\cosh(kH)}{\cosh(k'H)}\Phi^s_{1,\boldsymbol{k}'}(t)G_{\boldsymbol{k}-\boldsymbol{k}'}\mathrm{e}^{\mathrm{i}\boldsymbol{l}\cdot\boldsymbol{U}t}. \tag{2.44}$$

After calculations detailed in Appendix B (see Magne 2005 for further details), ϕ_2 yields the following contribution to the wave action,

$$N_{2,0}(\boldsymbol{k}) + N_{0,2}(\boldsymbol{k}) = -\frac{\pi t}{4\sigma}\int_0^{2\pi} M^2(\boldsymbol{k},\boldsymbol{k'})F^B(\boldsymbol{k}-\boldsymbol{k'})\frac{N_0(\boldsymbol{k})}{\sigma\sigma'}\frac{k'}{C_g}\frac{C_g+\boldsymbol{k}\cdot\boldsymbol{U}}{C'_g+\boldsymbol{k'}\cdot\boldsymbol{U}}\mathrm{d}\theta' + O(1), \tag{2.45}$$

in which $\sigma' = \sigma - \boldsymbol{l}\cdot\boldsymbol{U}$, $\sigma'^2 = gk'\tanh(kH)$ and $C'_g = \sigma'(1/2 + k'H/\sinh(2k'H))/k'$.

2.5. *Action and momentum balances*

The solvability condition for the spectral wave action at second order imposes that all secular terms cancel. Neglecting the first order energy contribution S_1 given by (2.31), and using $N(\boldsymbol{k}) = N_0(\boldsymbol{k})\,[1+O(\eta)]$ one has,

$$\frac{\mathrm{d}N(\boldsymbol{k})}{\mathrm{d}t} = S_{\mathrm{bscat}}(\boldsymbol{k}), \tag{2.46}$$

with the spectral action source term,

$$S_{\mathrm{bscat}}(\boldsymbol{k}) = \frac{\pi}{2}\int_{\theta'}\frac{M^2(\boldsymbol{k},\boldsymbol{k'})}{\sigma\sigma'}F^B(\boldsymbol{k}-\boldsymbol{k'})\left[N(\boldsymbol{k'})\frac{k'}{C'_g} - N(\boldsymbol{k})\frac{k'^2\,(kC_g+\boldsymbol{k}\cdot\boldsymbol{U})}{kC_g\left(k'C'_g+\boldsymbol{k'}\cdot\boldsymbol{U}\right)}\right]\mathrm{d}\theta', \tag{2.47}$$

where $\sigma' = \sigma + \boldsymbol{l}\cdot\boldsymbol{U}$ and $\boldsymbol{k} = \boldsymbol{k'} + \boldsymbol{l}$. This interaction rule was already given by Kirby (1988). The only waves that can interact share the same absolute frequency $\omega = \sigma + \boldsymbol{k}\cdot\boldsymbol{U} = \sigma' + \boldsymbol{k'}\cdot\boldsymbol{U}$. For a given $\boldsymbol{k}$ and without current, the resonant $\boldsymbol{k'}$ and $\boldsymbol{l}$ lie on circles in the wavenumber plane (see AH). The current slightly modifies this geometric property. For $U << C_g$ the circles become ellipses (Appendix C).

For a given value of ω, one may obtain the source term integrated over all directions,

$$\begin{aligned} S_{\mathrm{bscat}}(\omega) &= \int_\theta kS_{\mathrm{bscat}}(\boldsymbol{k})\frac{\partial k}{\partial\omega}\mathrm{d}\theta \\ &= \int_\theta\int_{\theta'}\frac{\pi}{2}\frac{M^2(\boldsymbol{k},\boldsymbol{k'})}{\sigma\sigma'}F^B(\boldsymbol{k}-\boldsymbol{k'})\left[\frac{k'k}{C'_g}\frac{\partial k}{\partial\omega}N(\boldsymbol{k'}) - \frac{k'k}{C_g}\frac{\partial k'}{\partial\omega}N(\boldsymbol{k})\right]d\theta'\mathrm{d}\theta. \end{aligned} \tag{2.48}$$

This expression is fully symmetric, and is thus unchanged when θ and θ' are exchanged. Thus $S_{\rm bscat}(\omega)$ is a substraction of two equal terms, so that for any bottom and wave spectra $S_{\rm bscat}(\omega) = 0$. In other words, the 'source term' is rather an 'exchange term', and conserves the wave action at each absolute frequency. This conservation is consistent with the general wave action conservation theorem proved by Andrews & McIntyre (1978), which states that there is no flux of action through an unperturbed boundary (here the bottom).

$S_{\rm bscat}$ may be re-written in a form close to that in AH,

$$S_{\rm bscat}(\boldsymbol{k}) = \int_{\theta'} K(k,k',H) F^B(\boldsymbol{k}-\boldsymbol{k'}) \left[N(\boldsymbol{k'}) - N(\boldsymbol{k}) \frac{k' C'_g \left(kC_g + \boldsymbol{k}\cdot\boldsymbol{U}\right)}{kC_g \left(k' C'_g + \boldsymbol{k'}\cdot\boldsymbol{U}\right)} \right] d\theta', \quad (2.49)$$

with

$$K(k,k',H) = \frac{4\pi\sigma k k'^3 \cos^2(\theta-\theta')}{\sinh(2kH)[2k'H + \sinh(2k'H)]}. \quad (2.50)$$

Finally, we may also write the evolution equation for the wave pseudo-momentum $\mathbf{M}^w = \rho_w g \int \boldsymbol{k} N(\boldsymbol{k}) \mathrm{d}\boldsymbol{k}$ (see Andrews & McIntyre 1978), where ρ_w is the density of sea water. For slow medium and wave field variations, that do not interfere with the scattering process, except by probably reducing the surface-bottom bispectrum Z, one obtains an extension of the equation of Phillips (1977)

$$\frac{\partial M^w_\alpha}{\partial t} + \frac{\partial}{\partial x_\beta}\left[(U_\beta + C_{g\beta}) M^w_\alpha\right] = T^{\rm bscat}_\alpha - M^w_\beta \frac{\partial U_\beta}{\partial x_\alpha} - \frac{M^w_\alpha}{k_\alpha} \frac{k\sigma}{\sinh 2kD} \frac{\partial D}{\partial x_\alpha}, \quad (2.51)$$

with the dummy indices α and β denoting dummy horizontal components, and the scattering stress vector,

$$\mathrm{T}^{\rm bscat} = \rho_w g \int \boldsymbol{k} S_{\rm bscat} \mathrm{d}\boldsymbol{k}. \quad (2.52)$$

This stress has dimensions of force per unit length and corresponds to the force necessary to compensate for the divergence of the wave pseudo-momentum flux. Based on the results of Longuet-Higgins (1967) and Hara & Mei (1987), this force does not contribute to the mean flow equilibrium with a balance of the radiation stresses divergence by long waves (or wave set-up in stationary conditions), contrary to the initial proposition of Mei (1985). This force is thus provided by a mean non-hydrostatic pressure on the bottom that correlates with the bottom slope, and must arise from the pressure under partial standing waves locked in phase with the bottom undulations.

3. Wave scattering in two dimensions

Before considering the full complexity of the 3D wave-bottom scattering in the presence of a current, we first examine the behavior of the source term in the case of 2D sinusoidal seabeds. MAHR have investigated the applicability limits of the source term with $U = 0$, using 2D test cases. They showed that for small bottom amplitudes the source term yields accurate reflection estimates, even for localized scatterers. It is thus expected that this also holds for $U \neq 0$, and that the present theory should conform to Kirby's (1988) theory in the limit of small reflection coefficients.

3.1. *Wave evolution equation in 2D*

We consider here a steady wave field in two dimension with incident and reflected waves propagating along the x-axis. We shall consider in particular the case of m sinusoidal

bars of amplitude b and height $2b$, defined by,

$$h(x) = b\sin(ml_0x) \quad \text{for} \quad 0 < x < L \tag{3.1}$$
$$h(x) = 0 \quad \text{otherwise.}$$

This form is identical to that of the bottom profile chosen by Kirby (1988) but differs, for $0 < x < L$, by a $\pi/2$ phase shift from the bottom profile chosen by Mei (1985). The bottom spectrum is thus

$$F^B(l_x, l_y) = F^{B2D}(l_x)\delta(l_y), \tag{3.2}$$

For this particular bottom

$$F^{B2D}(l) = \left(\frac{1}{2\pi}\int_{-\infty}^{\infty} h(x)\mathrm{e}^{-\mathrm{i}lx}\mathrm{d}x\right)^2 = \frac{2b^2l_0^2}{\pi L}\frac{\sin^2(lL/2)}{(l_0^2-l^2)^2}, \tag{3.3}$$

with

$$F^{B2D}(l_0) = \frac{mb^2}{4l_0} = \frac{b^2L}{8\pi}. \tag{3.4}$$

Please note that this is a double-sided spectrum, with only half of the bottom variance contained in the range $l > 0$. For a generic bottom, for which $h(x)$ does not go to zero at infinity, the spectrum is obtained using standard spectral analysis method, for example, from the Fourier transform of the bottom auto-covariance function (see MAHR).

First, replacing (3.2) in (2.46) removes the angular integral in the source term. Taking $\boldsymbol{k} = (k, 0)$, we have $l_y = -k'_y$, and

$$S_{\mathrm{bscat}}(\boldsymbol{k}, x) = K(k', k, H)\frac{F^{B2D}(\boldsymbol{k}-\boldsymbol{k'})}{k'}\left[N(\boldsymbol{k'}) - N(\boldsymbol{k})\frac{k'C'_g}{kC_g}\frac{kC_g + \boldsymbol{k}\cdot\boldsymbol{U}}{k'C'_g + \boldsymbol{k'}\cdot\boldsymbol{U}}\right]. \tag{3.5}$$

Second, assuming now that waves propagate only along the x-axis, the wave spectral densities are of the form

$$N(k_x, k_y) = N^{2D}(k_x)\delta(k_y). \tag{3.6}$$

Integrating over k_y removes the singularities on k_y, and assuming a steady state one obtains

$$\left[\frac{k_x}{k}C_g + U_x\right]\frac{\partial N}{\partial x}(k_x, x) = S_{\mathrm{bscat}^{2D}}(k_x, x), \tag{3.7}$$

with

$$S^{2D}_{\mathrm{bscat}}(k_x, x) = K(k', k, H)F^{B2D}(\boldsymbol{k}-\boldsymbol{k'})\left[\frac{N^{2D}(k'_x, x)}{k'} - N^{2D}(k_x, x)\frac{C'_g}{kC_g}\frac{kC_g + \boldsymbol{k}\cdot\boldsymbol{U}}{k'C'_g + \boldsymbol{k'}\cdot\boldsymbol{U}}\right]. \tag{3.8}$$

Although the present theory is formulated for random waves, the wave spectrum does not need to be continuous because there is no possible coupling between waves of different frequencies. We may thus express the result for monochromatic incident waves, such that, $N^{2D}(k, x) = N(x)\delta(k - k_0) + N'(x)\delta(k' - k'_0)$ with $k_0 > 0$ and $k'_0 < 0$. The resulting evolution equation is, omitting the 0 subscripts on k and k',

$$\left[\frac{k_x}{k}C_g + U_x\right]\frac{\partial N}{\partial x}$$
$$= K(k', k, H)\frac{F^{B2D}(\boldsymbol{k}-\boldsymbol{k'})}{k'}\left[N'\frac{k}{k'}\frac{k'C'_g + \boldsymbol{k'}\cdot\boldsymbol{U}}{kC_g + \boldsymbol{k}\cdot\boldsymbol{U}} - N\frac{k'C'_g}{kC_g}\frac{kC_g + \boldsymbol{k}\cdot\boldsymbol{U}}{k'C'_g + \boldsymbol{k'}\cdot\boldsymbol{U}}\right], \tag{3.9}$$

with a similar equation for N' obtained by exchanging C_g and C'_g, and k' and k, from which it is easy to verify that the total action is conserved.

The stationary evolution equation only couples two wave components $N(k)$ and $N(k')$. For a uniform mean depth H, and uniform bottom spectrum F^B, as considered here, we thus have a linear system of two differential equations, that may be written in matrix form for any $k > 0$,

$$\frac{\mathrm{d}}{\mathrm{d}x}\begin{pmatrix} N(k) \\ N(k') \end{pmatrix} = \mathsf{Q}\begin{pmatrix} N(k) \\ N(k') \end{pmatrix}. \tag{3.10}$$

The general solution is thus

$$\begin{pmatrix} N(k,x) \\ N(k',x) \end{pmatrix} = \mathrm{e}^{\mathsf{Q}x}\begin{pmatrix} N(k,0) \\ N(k',0) \end{pmatrix}, \tag{3.11}$$

and the reflection coefficient for the wave action is found using the boundary condition expressing the absence of incoming waves from beyond the bars, $N(k', L) = 0$, giving,

$$R_N = \frac{N(k',0)}{N(k,0)} = -\left(\mathrm{e}^{\mathsf{Q}x}\right)_{2,1} / \left(\mathrm{e}^{\mathsf{Q}x}\right)_{2,2}. \tag{3.12}$$

A reflection coefficient for the modulus of the wave amplitude predicted by the source term is thus,

$$R_S = \left[\frac{\sigma' N(-k',0)}{\sigma N(k,0)}\right]^{1/2} = -\left\{\sigma'\left(\mathrm{e}^{\mathsf{Q}x}\right)_{2,1} / \left[\sigma\left(\mathrm{e}^{\mathsf{Q}x}\right)_{2,2}\right]\right\}^{1/2} \tag{3.13}$$

3.2. *Analytical solution for $U = 0$*

If $U = 0$ then $k' = -k$, and

$$q = -Q_{1,1} = Q_{1,2} = -Q_{2,1} = Q_{1,1} = K(k,H)\frac{F^B(2k)}{C_g k}, \tag{3.14}$$

with $Q_{i,j}$ the (i,j) component of Q. Q is not diagonalizable, which would allow a simple way of evaluating the matrix exponential e^{Q}. However $\mathsf{Q}^2 = 0$ so that $\mathrm{e}^{\mathsf{Q}x} = (\mathsf{I} + \mathsf{Q})\,x$, where I is the identity matrix. The solution is thus simply,

$$N(k,x) = N(k,0)\left[\frac{-q\,(x-L)+1}{1+qL}\right] \tag{3.15}$$

$$N(-k,x) = N(k,0)\left[\frac{-q\,(x-L)}{1+qL}\right]. \tag{3.16}$$

An example of spatial variation of the wave spectrum from $x = 0$ to $x = L$ is shown in Figure 2, for $U = 0$, and a uniform (white) incident spectrum. The reflected wave energy (at $k < 0$ in figure 2.*a*) compensates the loss of energy in the transmitted spectrum (at $k > 0$ in figure 2.*b*).

At resonance, in the limit of small bar amplitudes (3.4) yields

$$R_S = (qL)^{1/2} + O(qL) = \frac{k^2 bL}{2kH + \sinh(2kH)} + O(qL) \tag{3.17}$$

which is identical to Mei's (1985) equation (3.21)–(3.22) for exact resonance, in the limit of $qL \ll 1$, and also converges to the result of Davies & Heathershaw (1984) for that same limit. For large bar amplitudes, the reflection is significant if the bars occupy a length L longer than the localization length $1/q$. However, the reflection coefficient for the wave amplitude only increases with L as $[qL/(1+qL)]^{1/2}$, which is slower than the

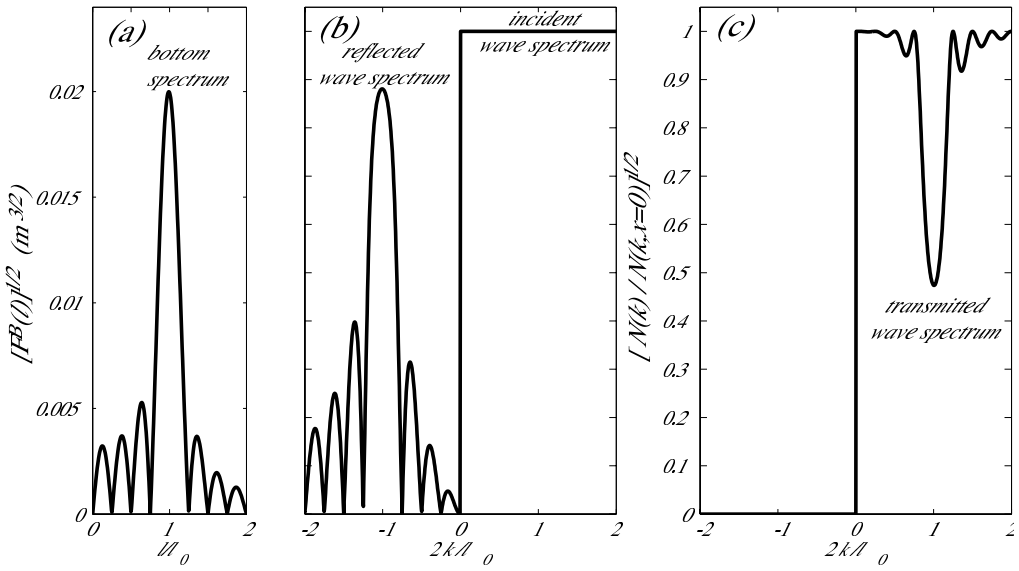

FIGURE 2. Bottom spectrum and evolution of a surface wave spectrum along a field of sinusoidal bars for $U = 0$, $b = 0.05$ m, $H = 0.156$ m, so that $b/H = 0.32$, and $l_0 = 2\pi$, $n = 4$, so that $L = 4\ m$ (bottom shown in figure 1). (a) square root of the bottom spectrum, (b) and (c) normalized square root wave spectrum upwave (at $x < 0$) and downwave (at $x > L$) of the bars, respectively. The incident spectrum ($k > 0$ at $x = 0$) is specified to be white (unform in wavenumbers).

exponential asymptote given by Mei (1985) for sinusoidal bars, and predicted by (Belzons *et al.* 1988) from the lowest-order theory applied to a random bottom. Our use of higher-order correction may be thought as the representation of multiple reflections that tend to increase the penetration length in the random medium.

A deeper understanding of this question is provided by the comparison of numerical estimations of the reflection coefficients for the wave amplitudes R. A benchmark estimation for linear waves is provided by the step-wise model of Rey (1995) using integral matching conditions for the free propagating waves and three evanescent modes at the step boundaries. This model is known to converge to the reflection coefficents given by an exact solution of Laplace's equation and the boundary conditions, in the limite of an infinite number of steps and evanescent modes. Calculations are performed here with 70 steps. This number is chosen because a larger number of steps gives indistinguishable results in figure 3. An analytical expression R_{Mei} is given by Mei (1985). R for the present second order theory is given by R_S (3.13).

We further compare these estimates to the reflection coefficient $R_{S1,\mathrm{Mei}}$ that is deduced from the energy evolution given by Hara & Mei (1987) using the approximate solutions of Mei (1985, his equations 3.8–3.23). One may prefer to reformulate the energy evolution from the amplitude evolution equations of Kirby (1988) because he used a continuous water depth $h = \sin(ml_0)$, instead of Mei's $h = \cos(ml_0)$ which is discontinuous at $x = 0$ and $x = L$†. Yet both Mei's and Kirby's equations lead to the same energy exchange between the incident and reflected components. Using Mei's (1985) notations, the amplitudes of the incident waves, reflected waves, and bottom undulations are $A =$

† Such a discontinuous bottom has a markedly different spectrum at low and high frequencies. The present theory, confirmed by calculations with Rey's (1995) numerical model, yield very different reflection coefficients for waves much shorter and much longer than the resonant waves

$2\sigma\Phi^+_{0,\boldsymbol{k}}/g$, $B = 2\sigma\Phi^-_{0,\boldsymbol{k}}/g$, and $D = -2\mathrm{i}G_{-2k}$, and the 'cut-off' frequency is

$$\Omega_0 = \frac{\sigma k D}{2\sinh(2kH)}. \tag{3.18}$$

The energy evolution of waves propagating over sinusoidal bars along the x-axis is given by Hara & Mei (1987). The reflected wave energy $BB^\star/2$ should be a solution of

$$\frac{\partial}{\partial t}\left(\frac{BB^\star}{2}\right) - C_g\frac{\partial}{\partial x}\left(\frac{BB^\star}{2}\right) = S_{1,\mathrm{Mei}} = \mathrm{Re}\left(\mathrm{i}\Omega_0 B^\star A\right), \tag{3.19}$$

where $B^\star$ denotes the complex conjugate of B. This is identical to (2.30) for a *monochromatic* bottom except that the imaginary part replaced by a real part.

Equation (3.19) yields a corresponding energy reflection coefficient, given by the fraction of energy lost by the incoming waves,

$$R_{E,S1\mathrm{Mei}} = -\frac{1}{C_g}\int_0^L S_{1,\mathrm{Mei}}(x)\mathrm{d}x. \tag{3.20}$$

Simple analytical expressions can be obtained at resonance, where Mei's (1985) eq. (3.20)–(3.21) give,

$$\frac{AB^\star}{A^2(0)} = \frac{-\mathrm{i}\sinh\left(2\tau(1-x/L)\right)}{2\cosh^2\tau} \tag{3.21}$$

so that

$$R_{E,S1\mathrm{Mei}} = \frac{\cosh 2\tau - 1}{4\cosh^2\tau} = \frac{1}{2}\tanh^2\tau = \frac{1}{2}R^2_{\mathrm{Mei}}, \tag{3.22}$$

and

$$R_{S1,\mathrm{Mei}} = 2^{-1/2}R_{\mathrm{Mei}}. \tag{3.23}$$

It is not surprising that the energy transfer thus computed differs from the energy computed from the amplitude evolution equations. This is typical of small perturbation methods, and was discussed by Hasselmann (1962), among others. Yet, it is remarkable that the ratio of the two is exactly one half. The transfer of energy given by $\mathrm{i}\Omega_0 B^\star A$ in (3.19) thus correspond to an amplitude reflection coefficient $R_{S1,\mathrm{Mei}}$ that is smaller by a factor $2^{-1/2}$, at resonance, compared to R_{Mei} (figure 3). This underprediction of the the reflexion of the energy by (3.22) also has consequences for the analysis and calculation of wave set-up due to wave group propagation over a reflecting bottom. Indeed, the estimation of the scattering stress (2.52), that contribute to the driving of long waves, was analyzed by Hara & Mei (1987) using (3.22), which is a factor 2 too small. This may explain, in part, their under-prediction of the observed elevation of the long wave travelling with the incident wave group.

3.3. *Effects of wave and bottom relative phases*

The energy exchange coefficient given by the source term always gives energy to the least energetic components (in the absence of currents), and thus the energy evolution is monotonic. However, the first order term that was neglected so far may have any sign, and thus lead to oscillatory evolutions for the wave amplitudes, as predicted by Mei (1985) and observed by Hara & Mei (1987). At resonance, and for $U = 0$, it can be seen that the first-order energy product $\Phi^+_{0,\boldsymbol{k}}\Phi^-_{0,\boldsymbol{k}}G_{-2k}$ in (2.30) is equal to $\mathrm{i}AB^\star D/8$, in the limit of a large number of bars. Based on Mei's (1985) approximate solution, in the absence of waves coming from across the bars, this quantity is purely real so that its imaginary part is zero and the corresponding reflection coefficient R_{S1} is zero. For $U \neq 0$ this property remains as can be seen by replacing Mei's (1985) solution with Kirby's (1988). However,

similar correlation terms were also neglected in the second order energy, so that the oscillatory behaviour may occur due to terms of the same order as the scattering source term, including interactions of the sub-harmonic kind (Guazzelli *et al.* 1992). Further, the bottom-surface bispectrum may become significant in the first order term if there is a large amount of wave energy coming from beyond the bars. This kind of situation, e.g. due to reflection over a beach, was discussed by Yu & Mei (2000).

In the absence of such a reflection, and away from resonance but for small values of the scattering strength parameter $\tau = (qL)^{1/2} = \Omega_0 L/C_g$, the imaginary part of $\Phi^+_{0,\boldsymbol{k}}\Phi^-_{0,\boldsymbol{k}}G_{-2k}$ is an order $(qL)^{1/2}$ smaller than the real part and thus contributes a negligible amount to the reflection.

3.4. *Source term and deterministic results for sinusoidal bars*

For large bar amplitudes, such as $b/H = 0.32$ (figure 3.*a*), all theories with linearized bottom boundary conditions fail to capture the shift of the reflection pattern to lower wavenumbers. This effect was discussed by Rey (1992), and attributed to the non-linear nature of the dispersion relation and the rapid changes in the water depth. However reflection coefficients are still relatively well estimated. For these large amplitudes Mei's (1985) approximate solution is found to be more accurate at resonance compared to the source term. As expected from MAHR, $R_{\rm Mei}$ and R_S become identical as $\eta = b/H$ goes to zero (figure 3.*b*). This fact provides a verification that the first order term S_1 is different from Hara and Mei's (1987) energy transfer term, and only accounts for a small fraction of the reflection, a fraction that goes to zero as $\eta \to 0$. It is also found that for all bottom amplitudes, but away from resonance, the source term expression provides a simple solution that is more accurate than Mei's (1985) approximate solutions (see the sidelobes in figure 3).

3.5. *Effects of currents*

The basic feature of the solutions with currents is the modification of the resonant condition from $k = k'$ and $l = 2k$, to $\sigma' = \sigma + lU$ and $l = k + k'$. Notations here assume that $\boldsymbol{k}$ is in the direction of the current and $\boldsymbol{k}'$ is opposite to the current. Yet, the introduction of the current makes the solution much more complex. It is striking that Kirby's (1988) equations involve a modified cut-off parameter $\Omega_c = \Omega_{0c} + \Omega_{1c}$, which is analytically similar to our source term result except for the rather complicated Ω_{1c} term. At resonance, Kirby (1988) found that the transmission losses $1-T$ differ from the case without current. In the long-wave limit this difference is increased by a factor $\left(1 - Fr^2\right)^{-1}$ (his equation 5.29). However, the present theory predicts an increase by a factor $1 + Fr$. Thus both theories only agree in the limit $Fr \to 0$. To our knowledge there is unfortunately no simple numerical method to arrive at an independent solutions. Besides, observations of that effect require to test relatively large Froude numbers. Some first observations of the shift in resonant frequencies in the presence of currents were only performed at relatively low Froude numbers, and are not accurate enough to test these predictions (Magne, Rey & Ardhuin manuscript submitted to Physics of Fluids).

We now compare reflection coefficients for monochromatic waves, as obtained with the source term using (3.9), and with Kirby's (1988) analytical approximate solutions for near-resonant waves. An approximation to the reflection coefficient (3.13) corresponding to the solution of (3.9) is obtained with a fourth order Taylor expansion of the matrix exponential. Anticipating oceanographic conditions with a water depth of 20 m, a strong 2 m s^{-1} current corresponds to a Froude number of 0.17 only. For such a low value of Fr in the context of the Davies & Heathershaw (1984) laboratory experiments, the difference in peak reflection for $b/H = 0.065$ is of 8% only between the source term and Kirby's

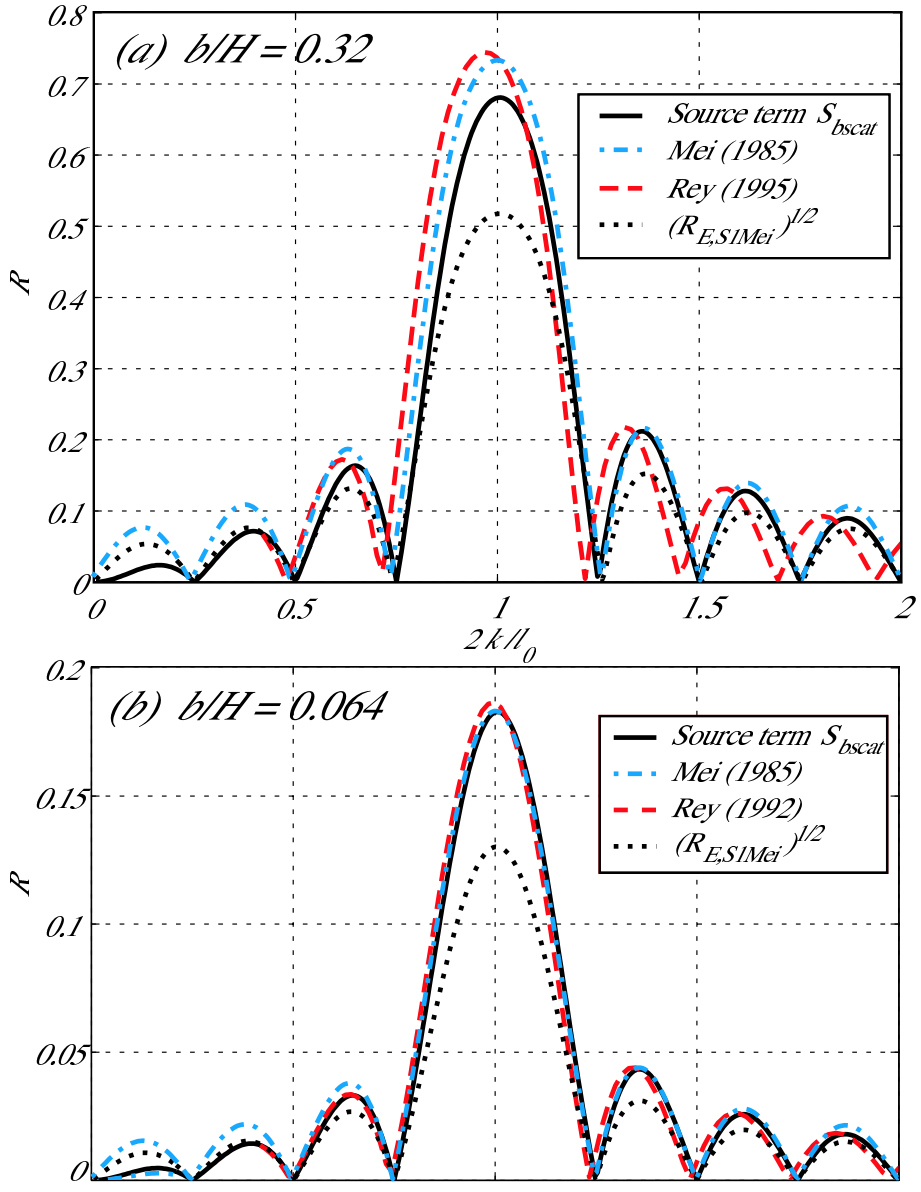

FIGURE 3. Reflection coefficients for the wave amplitudes for $U = 0$, $H = 0.156$ m, $l_0 = 2\pi$, $n = 4$. In (a) $b = 0.05$ so that $b/H = 0.32$, corresponding to one of the experiments of Davies & Heathershaw (1984), and in (b), $b = 0.01$, so that $b/H = 0.064$.

(1988) solution, while the reflection coefficient is largely increased due to the general conservation of the wave action flux. R can thus be larger than 1 for currents following the incident waves because it is enhanced by the factor $\{\sigma(Cg + U)/[\sigma'(Cg' - U)]\}^{1/2}$, compared to the transmission losses $1 - T$. The overall increase in R for following waves amounts to about 60% at $Fr = 0.17$, for the laboratory sinusoidal bars of Davies & Heathershaw (1984) shown before (figure 4). The horizontal density of reflected wave energy is thus multiplied by a factor 2.5 in this case, for a Froude number of only 0.17.

Both solutions agree reasonably well, and we thus expect the source term to represent

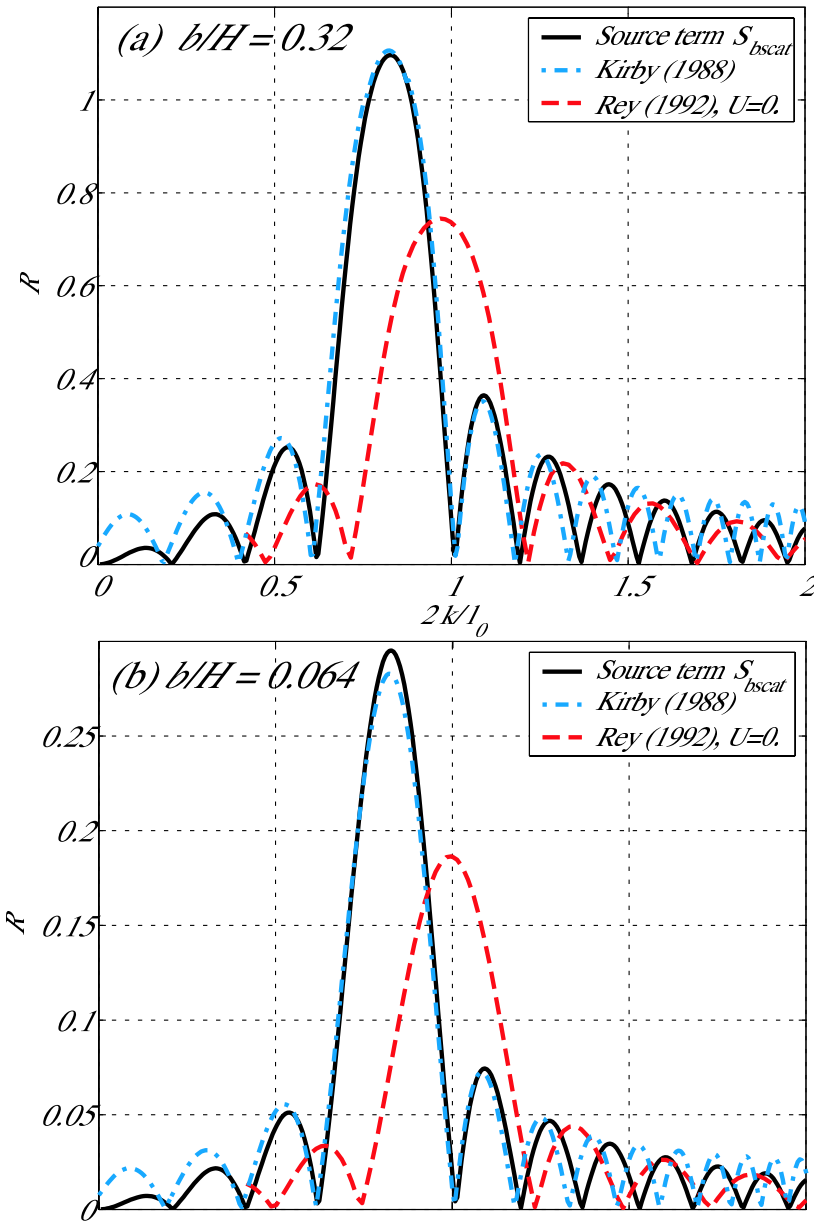

FIGURE 4. Amplitude reflection coefficients for monochromatic waves over sinusoidal bars for the same settings as in figure 3 with $U = 0.2$ m s^{-1}. For reference the reflection coefficient without current, as given by the exact model of Rey (1995), is also shown.

accurately the scattering of waves over bottom topographies in cases of uniform currents. For four sinusoidal bars the energy reflection coefficients was found to be within 20% of the exact solution for $\eta < 0.2$ and $Fr = 0$, and this conclusion is expected to hold for $Fr < 0.2$, given the agreement with Kirby's (1988) approximate solution. This accuracy is a factor two better than what was found for a rectangular step with $Fr = 0$ (MAHR). The present method has the advantage of a large economy in computing power. This method is also well adapted for natural sea beds, for which continuous bathymetric coverage is

only available in restricted areas, and thus only the statistical properties of the bottom topography are accessible, assuming homogeneity.

4. Scattering with current on a realistic topography

4.1. *Sandwaves in the North Sea*

A real ocean topography, at least on the continental shelf, generally presents a continuous and broad bottom elevation spectrum. Given this bottom spectrum, simple solutions are available for uniform conditions, because the scattering source term is a linear function of the directional spectrum at a given value of the absolute frequency ω (see AH for numerical methods). However, practical situations rather correspond to quasi-stationary conditions with spatial gradients in at least one dimension. In this situation the simple steady solutions found above for 2D topography are not physical. Indeed, a 3D bottom causes scattering along the transversal direction y, and the energy propagating in that direction builds up slowly up to the point where it becomes as large as the incident wave energy. This process can take a time much longer than the typical duration of a storm or swell arrival, and dissipative processes are likely to be important as the wave energy increases (e.g. Ardhuin *et al.* 2003).

Therefore the source term $S_{\rm bscat}$ was introduced in the version 2.22 of the wave model WAVEWATCH-III (Tolman 2002), based on the wave action evolution equation (2.46) in which the time derivative on the left hand side is now a Lagrangian derivative following a wave packet in physical and spectral space. Bottom scattering is the only source term introduced in the present calculation. There is thus no transfer of wave action between frequencies. However, the model uses a spectrum is discretized with components at fixed intrinsic frequencies σ and directions θ, which is most appropriate for other processes. Thus, the model was run with a typical grid of 25 frequencies ranging from 0.08 to 0.788 Hz and a high directional resolution of 3°.

The effects of a mean current on wave scattering are now examined using a real bathymetry spectrum that is estimated from a detailed bathymetric survey of an area centered on the crest of a sand dune, in the southern North Sea (figure 5). In this region, tidal currents are known to generate a wide array of bedforms, from large scale tidal Banks to sand dunes and sand waves (e.g. Dyer & Huntley 1999; Hulscher & van den Brink 2001). Although sand dunes present a threat to navigation and are closely monitored (Idier *et al.* 2002), dunes are much larger than typical wind seas and swells wavelengths. These dunes, however, are generally covered with shorter sandwaves. In the surveyed area the sandwaves have a peak wavelength of 250 m, and a variance of 1.7 m^2, which should lead to strong oblique scattering of waves with periods of 10 s and longer. Over areas of 3 by 3 km the variance can be as large as 3.3 m^2 with a better defined spectral peak, so that our chosen spectrum is expected to be representative of the entire region, including high and low variances on dunes crests and troughs, respectively. The southern North Sea is also known for the attenuation of long swells, generated in the Norwegian Sea. This attenuation has been generally attributed to the dissipation of wave energy by bottom friction (Weber 1991).

The bottom spectrum of the area that we chose, like the spectra that were obtained by AH from the North Carolina shelf, roll off sharply at high wavenumbers, typically like l^{-4} for the two-dimensional spectrum. Here the maximum variance is found for bottom wavelengths of the order or larger than 250 m (figure 5). For a typical swell period of 10 s, this corresponds to 2 times the wavelength in 20 m depth, and thus a rather small scattering angle, 30° off from the incident direction. Swells propagating from a distant

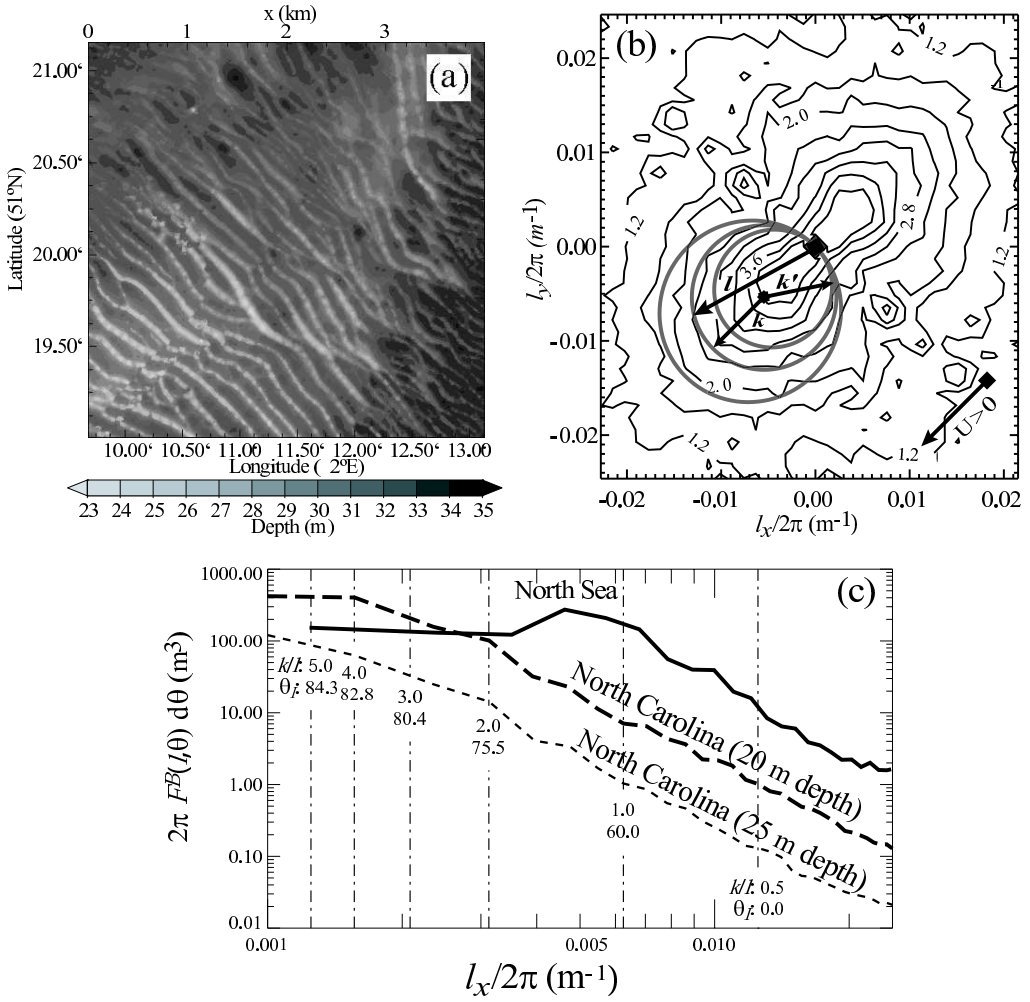

FIGURE 5. (a) high-resolution bathymetry of a sand wave field in the southern North Sea with depths relative to chart datum, and (b) corresponding bottom elevation spectrum with contour values representing $\log_{10}\left(4\pi^2 F^B\right)$. The locus of the interacting bottom and surface wave components are indicated for a 12.5 s waves from the North-East in 25 m depth, with $U = 0$ (middle circle), $U = 2$ m s^{-1} (smaller ellipse), and $U = -2$ m s^{-1} (larger ellipse), U is positive from the North-East. (c) Direction-integrated bottom variance spectra from the North Carolina shelf and the southern North Sea. Vertical lines indicate k/l ratios and incident resonant directions θ_I, assuming an incident wave field of 12.5 s period in 25 m depth and bedforms parallel to the y-axis. For such bedforms, the angle between incident and scattered waves is $180^\circ - 2\theta_I$.

storm, with fixed absolute frequency $\omega = \sigma + \boldsymbol{k} \cdot \boldsymbol{U}$, should be reflected by bottom undulations with widely different variances as the current changes.

4.2. *Scattering of waves normally incident on the sandwaves*

To simplify the interpretation of the results, and the processing of the boundary conditions, a one dimensional (East/West) propagation grid is used for the computations, assuming that the wave field, still fully directional, is uniform in the North-South direction. The waves are propagated over a model grid 100 km long, with a mean depth

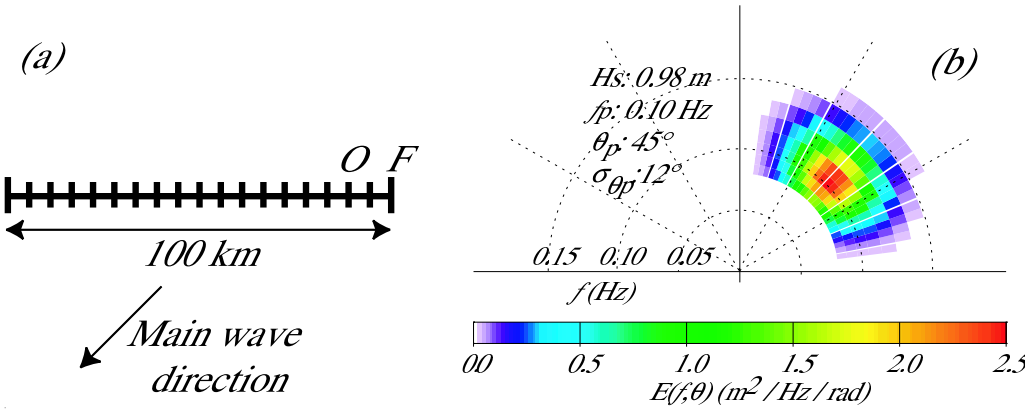

FIGURE 6. (a) Schematic of the model grid and (b) incident wave spectrum specified at point F. Model output is shown below for point O. Please note that waves are represented with their arrival direction (direction from, contrary to the standard wind sea convention). The frequency is the relative frequency $\sigma/2\pi$.

of 20m, and a spatial grid step of 5 km (figure 6.a). As a result, scattering is probably stronger than in real conditions where the mean water depth is typically larger than 20 m. The following results should still provide some understanding of the likely real effects, at least for larger wave periods with similar values of kH.

A Gaussian incident surface wave spectrum is imposed, with a mean direction from the North-East, a narrow peak directional spread of 12°, and a peak frequency of 0.01 Hz (figure 6.b). The source term is integrated with a time step of 120 s, and the advection in space uses a third order scheme with a time step of 120 s.

The scattering source term acts as a diffusion operator with a typical 3-lobe structure, negative at the peak of the wave spectrum, and positive in directions of about 30° on both sides of the peak. This is identical, but with a larger magnitude, to the effect described by AH. In general the scattering effects are relatively stronger at the lowest frequencies, at least in the range of frequencies used here. For still lower frequencies the scattering coefficient K decreases (see also AH) so that, on these spatial scales, very little scattering occurs for infra-gravity waves ($f < 0.05$ Hz). In addition to this grazing-angle forward scattering the present case shows a significant back-scattering, in particular in the case of following currents.

For a wave frequency of 0.08 Hz, the curves followed by the bottom resonant wavenumbers are overlaid on the bottom spectrum (figure 5.b). The wavenumbers $\boldsymbol{l}$ along these curves satisfy both the relations $\boldsymbol{k'} + \boldsymbol{l} = \boldsymbol{k}$ and $\sigma' = \sigma + \boldsymbol{l} \cdot \boldsymbol{U}$. Without current the curve is exactly a circle, and transforms to an ellipse for weak currents (Appendix C). This approximation is used in the model to compute the source term. The current shifts significantly the resonant configuration for the bottom and surface wavenumbers. A current opposed to the waves enlarges the ellipse towards higher wavenumbers, while a following current will lead to a 'sampling' of shorter wave numbers and longer bottom features. Since the bottom topography has the lowest variance at the largest wavenumbers, the scattering is strongest for following currents (figure 7). With our choice of parameters, there is about a factor 10 reduction in the bottom variance that causes backscatter as U is changed from 2 m s^{-1} to -2 m s^{-1}. Besides, as in the 2D case discussed above, the coupling coefficient $K(k', k, H)$ is increased in the case of a following current. Furthermore, a current opposed to the waves decreases the surface waves wavelength and favours resonant configuration such as $2k/l > 1$ corresponding to forward-scattering, so

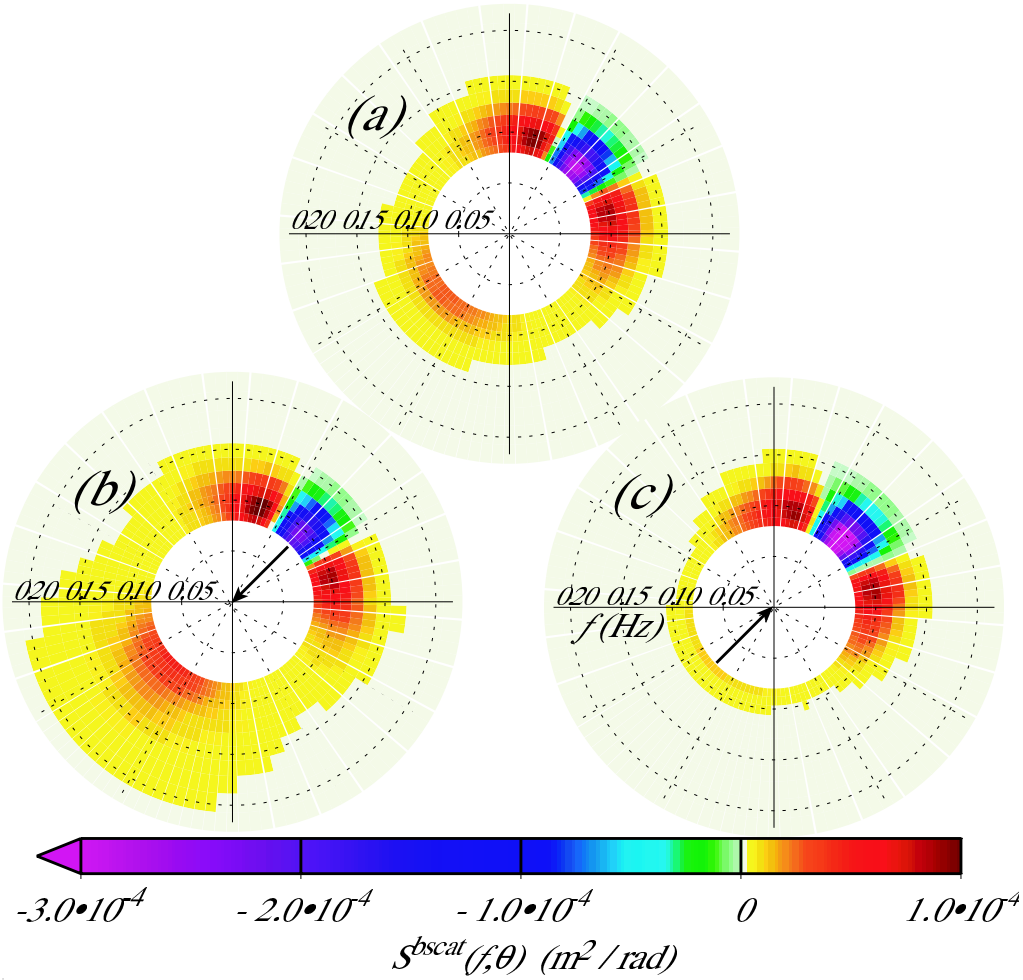

FIGURE 7. Computed source terms at the boundary forcing point F, (a) for $U = 0$, (b) for a following current $U = 2$ m s^{-1}, (c) for an opposing current $U = -2$ m s^{-1}. The frequency is the relative frequency $\sigma/2\pi$.

that the 3 lobes in the source term occupy a broader range of directions in the case of opposing currents.

The resulting wave spectra are further modified due to the conservation of the wave action flux. For $U > 0$ the reflected wave energies are enhanced (figure 8). This effect is similar to what was found in the 2D cases considered above, due to the different energy flux velocities $U + C_g$ for the incident waves, and $U - C'_g$ for the reflected waves. In all cases investigated here, the narrow incident wave spectrum is significantly broadened in directions, and that effect is most pronounced at the lowest frequencies. Without current or with following currents, spectra at the beginning of the model domain (figure 8) contain a large back-scattered energy, which increases the significant wave height and the directional spread on the up-wave side of the sandwave field. This effect should not be very sensitive to the directional spread of the incident wave field and should thus occur for a wide range of sea states. In contrast, it should be noted the initial spectral peak in figure (figure 8) is not much modified, because of the relatively short propagation distance from the forcing point (figure 6.*a*). Nevertheless, a significant broadening is predicted at

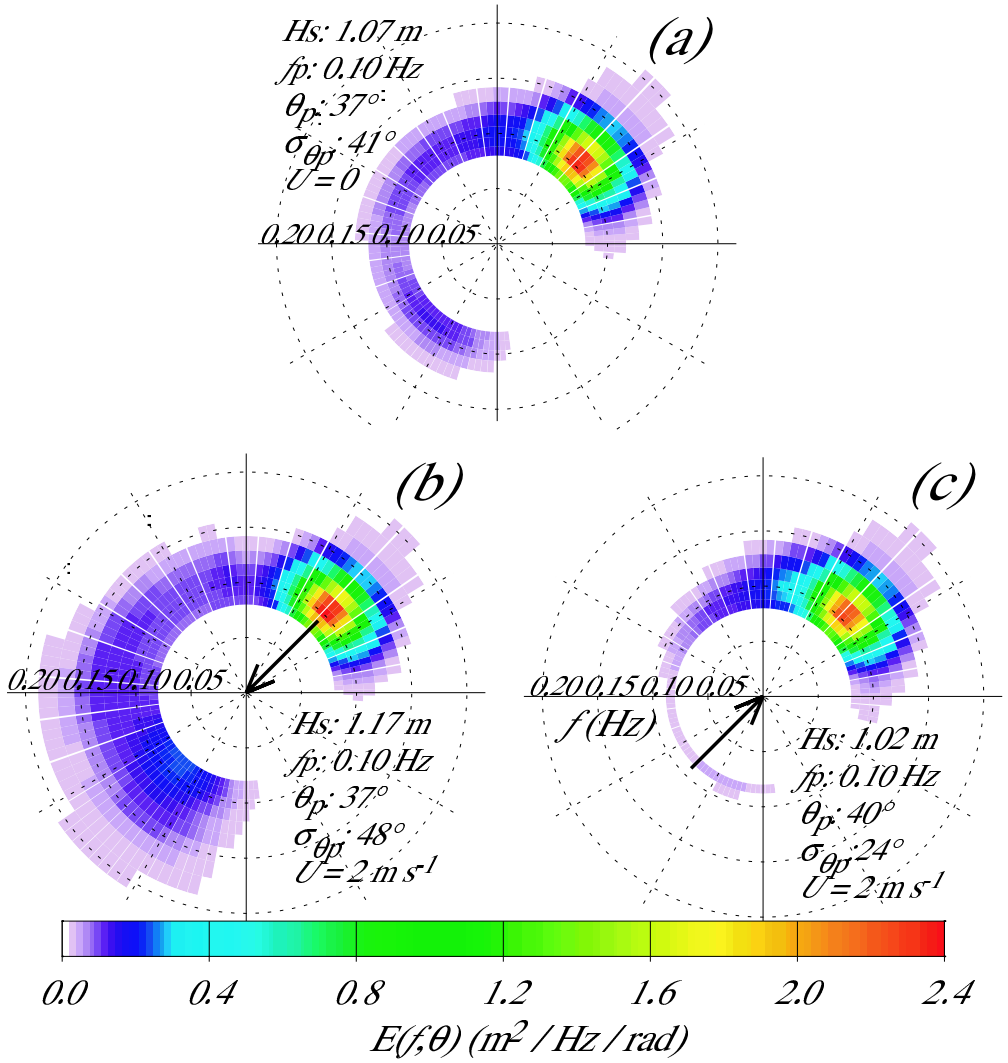

FIGURE 8. Computed wave spectra at point O, 10 km inside of the model domain, after 5 hours of propagation, (a) for $U = 0$, (b) for a following current $U = 2$ m s^{-1}, (c) for an opposing current $U = -2$ m s^{-1}. The frequency is the relative frequency $\sigma/2\pi$.

the down-wave end of the model domain, with values of the directional spreads σ_{theta} larger than 35° in all cases considered here. That broadening effect is small for relatively broad incident spectra (i.e. directional spreads $\sigma_{theta} > 30°$), as found by Ardhuin et al. (2003a) and Ardhuin and Herbers (2005). It was also found that this broadening of the main spectral peak is largest for waves propagating along the main sandwave crest directions (i.e. from the North-West in our case) due to the larger bottom variance at $\boldsymbol{l} = \boldsymbol{k} - \boldsymbol{k}'$ with $\boldsymbol{k} \simeq \boldsymbol{k}'$ (Magne 2005), with a significant modification of the mean direction.

Finally, a wave height decrease along the grid is observed, indicating an attenuation due to wave-bottom scattering. In reality, bottom friction would likely induce a stronger decay, and that decay would be stronger than in the absence of scattering. Essentially the scattering increases the average time taken by wave energy to cross the domain, and

bottom friction together with scattering would lead to a larger dissipation than friction alone because of that longer time (Ardhuin *et al.* 2003).

5. Conclusion

The effect of a uniform current on the wave-bottom Bragg scattering was investigated theoretically, extending the derivations of Ardhuin & Herbers (2002). After Magne *et al.* (2005) showed that the source term was applicable to non-random topography and accurate in the limit of small bottom amplitudes, it is found here that the source term is also applicable to monochromatic waves. Indeed, there is no process capable of coupling waves with different frequencies. For small bottom amplitudes the source term may only be inaccurate for non-stationary conditions, in which case the generation of the local bound waves requires some energy not explicitly evaluated by the present theory. The two scale approximation was found to hold reasonably well, even for a relatively fast evolution of the wave amplitudes over two wavelengths (figure 3). For a sinusoidal bottom and monochromatic waves, the source term converges to Mei's (1985) theory in absence of current and in the limit of the small bottom amplitudes. In the presence of a current, monochromatic wave results generally agree with Kirby's (1988) theory, but only converge in the limit of small Froude numbers. In two dimensions, the main effect of a current is a Doppler-like shift of the resonant wave frequencies that undergo maximum reflection. For a given bottom topography this leads to a modification of the wave reflection coefficient that is sensitive to the current strength and direction.

In three dimension and over the shallow areas of the southern North Sea, where large sand waves are found with strong tidal currents, wave scattering is expected to be significant, and largely influenced by currents. Over natural topographies, the bottom typically de-correlates over scales shorter than the scattering-induced attenuation scales, so that a modification of the reflection due to a phase locking of the incident and reflected waves with the bottom may be neglected. The wave scattering theory presented in this paper is thus one more piece in the puzzle of wave propagation over shallow continental shelves, and this process may account for a significant part of the observed attenuation of swells in the southern North Sea. Our representation of this phenomenon with a source term in the wave action balance equation is expected to be accurate in many conditions of interest. It is consistent with the wide use of phase-averaged models for engineering and scientific purposes when such large scales are involved. The alternative use of phase-resolving elliptic refraction-diffraction models (e.g. Berkhoff 1972 or Belibassakis et al. 2001), is much more expensive in terms of computer resources, due to the necessity to resolve the wave phase, and may not be much more accurate.

This research was supported by a joint grant from CNRS and DGA. Bathymetric data was acquired by the French Hydrographic and Oceanographic Service (SHOM). Discussions with Michael McIntyre, Kostas Belibassakis, Vincent Rey, and Thierry Garlan and gratefully acknowledged.

Appendix A. Harmonic oscillator equation for the first order potential

The harmonic oscillator equation (2.21) can be written as a linear superposition of equations of the type

$$\frac{d^2 f_1}{dt^2} + \omega^2 f_1 = \mathrm{e}^{\mathrm{i}\omega' t}. \tag{A 1}$$

In order to specify a unique solution to (A 1), initial conditions must be prescribed. In the limit of the large propagations distances, the initial conditions contribute a negligible bounded term to the solution. Following Hasselmann (1962), we choose $f_1(0) = 0$ and $df_1/dt(0) = 0$, giving the solution

$$f_1(\omega, \omega'; t) = \frac{\mathrm{e}^{\mathrm{i}\omega' t} - \mathrm{e}^{\mathrm{i}\omega t} + i(\omega - \omega')\sin(\omega t)/\omega}{\omega^2 - \omega'^2} \text{ for } \omega'^2 \neq \omega^2, \tag{A 2}$$

$$f_1(\omega, \omega'; t) = \frac{t\mathrm{e}^{\mathrm{i}\omega' t}}{2i\omega'} - \frac{\sin' \omega t)}{2i\omega'\omega} \text{ for } \omega' = \pm\omega \tag{A 3}$$

Appendix B. Harmonic oscillator equation and energy for the second order potential

Replacing ϕ_1 (2.18) in the surface boundary condition (2.42),

$$\left(\frac{d^2}{dt^2} + \sigma^2\right) \Phi^s_{2,\boldsymbol{k}}(t) = -gk\Phi^{si,s}_{2,\boldsymbol{k}} - \tanh(kH)\frac{\partial^2 \Phi^{si,s}_{2,\boldsymbol{k}}}{\partial t^2}, \tag{B 1}$$

and conserving only the non-bounded terms of $\Phi^s_{1,\boldsymbol{k}'}$, one obtains

$$\frac{\partial^2 \Phi^{si,s}_{2,\boldsymbol{k}}}{\partial t^2} = \\ -\sum_{\boldsymbol{k}',\boldsymbol{k}''} \frac{\boldsymbol{k}'\cdot\boldsymbol{k}}{k} \frac{\cosh(kH)}{\cosh(k'H)} M(\boldsymbol{k}', \boldsymbol{k}'') G_{\boldsymbol{k}-\boldsymbol{k}'} G_{\boldsymbol{k}'-\boldsymbol{k}''} \Phi_{0,\boldsymbol{k}''} \frac{\partial^2}{\partial t^2}\left(f_1(\sigma', \boldsymbol{k}'\cdot\boldsymbol{U} - s\omega'')\mathrm{e}^{\mathrm{i}\boldsymbol{l}\cdot\boldsymbol{U}t}\right). \tag{B 2}$$

The amplitude $\Phi^s_{2,\boldsymbol{k}}$ satisfies a forced harmonic oscillator equation. Anticipating that only $k'' = k$ will give a non-zero contribution due to the correlation $G_{\boldsymbol{k}-\boldsymbol{k}'} G_{\boldsymbol{k}'-\boldsymbol{k}''}$, we may simplify the notations in that equation as,

$$\left(\frac{\partial^2}{\partial t^2} + \sigma^2\right) \Phi^s_{2,\boldsymbol{k}}(t) \\ = \sum_{\boldsymbol{k}'}\sum_{\boldsymbol{k}''} MM(\boldsymbol{k}', \boldsymbol{k}'') G_{\boldsymbol{k}-\boldsymbol{k}'} G_{\boldsymbol{k}'-\boldsymbol{k}''} \Phi_{1,\boldsymbol{k}''} f_1(\sigma', -\boldsymbol{l}'\cdot\boldsymbol{U} - s\sigma'')\mathrm{e}^{\mathrm{i}\boldsymbol{l}\cdot\boldsymbol{U}t}, \tag{B 3}$$

with $\boldsymbol{l}' = (\boldsymbol{k}'' - \boldsymbol{k}')\cdot\boldsymbol{U}$, and

$$M' = \frac{\boldsymbol{k}'\cdot\boldsymbol{k}}{k}\left[gk - \left(\sigma''^2 - (\sigma' + \boldsymbol{l}\cdot\boldsymbol{U})^2\right)\tanh(kH)\right]\frac{\cosh(kH)}{\cosh(k'H)}. \tag{B 4}$$

The second order potential potential amplitude must verify the equation

$$\left(\frac{d^2}{dt^2} + \sigma^2\right) \Phi^s_{2,\boldsymbol{k}}(t) = \sum_{\boldsymbol{k}'}\sum_{\boldsymbol{k}''} M'M(\boldsymbol{k}', \boldsymbol{k}'') G_{\boldsymbol{k}-\boldsymbol{k}'} G_{\boldsymbol{k}'-\boldsymbol{k}''} \Phi_{0,k} f_1(\sigma', -\boldsymbol{l}'\cdot\boldsymbol{U} - s\sigma'')\mathrm{e}^{\mathrm{i}\boldsymbol{l}\cdot\boldsymbol{U}t}, \tag{B 5}$$

thus we have to solve,

$$\left(\frac{d^2}{dt^2} + \sigma^2\right) f_2 = f_1(\sigma', -\boldsymbol{l}'\cdot\boldsymbol{U} - s\sigma'')\mathrm{e}^{\mathrm{i}\boldsymbol{l}\cdot\boldsymbol{U}t}. \tag{B 6}$$

The solution f_2 may be written as

$$f_2 = f_{2,a} + f_{2,b}, \tag{B 7}$$

where

$$f_{2,a} = -\frac{t\mathrm{e}^{-is\sigma'' t} - \sin(\sigma'' t)/\sigma''}{2is\sigma''\left[\sigma'^2 - (\boldsymbol{l'}\cdot\boldsymbol{U} + s\sigma'')^2\right]}, \tag{B 8}$$

$$f_{2,b} = -\frac{s}{2\sigma'(\sigma' - \left[\boldsymbol{l'}\cdot\boldsymbol{U} + s\sigma''\right]))} \times \left[\frac{\mathrm{e}^{-i(\sigma' - \boldsymbol{l'}\cdot\boldsymbol{U})t}}{\sigma''^2 - (\sigma' - \boldsymbol{l'}\cdot\boldsymbol{U})^2} - \frac{1}{2\sigma}\left(\frac{\mathrm{e}^{\mathrm{i}\sigma'' t}}{\sigma'' + (\sigma' - \boldsymbol{l'}\cdot\boldsymbol{U})} + \frac{\mathrm{e}^{-i\sigma'' t}}{\sigma'' - (\sigma' - \boldsymbol{l'}\cdot\boldsymbol{U})}\right)\right] \tag{B 9}$$

The second order energy contribution from correlation between the zeroth and first order velocity potential is given by,

$$F^{\Phi}_{2,0,\boldsymbol{k}} = F^{\Phi}_{0,2,\boldsymbol{k}} = 2\langle\phi^{+}_{2,\boldsymbol{k}}\phi^{-}_{0,-\boldsymbol{k}}\rangle. \tag{B 10}$$

Then (B 3) becomes

$$\frac{F^{\Phi}_{2,0,\boldsymbol{k}}}{\Delta\boldsymbol{k}} = \sum_{\boldsymbol{k'}}\sum_{\boldsymbol{k''}} M^2(\boldsymbol{k},\boldsymbol{k'})\frac{\langle G_{\boldsymbol{k}-\boldsymbol{k'}}G_{\boldsymbol{k'}-\boldsymbol{k''}}\rangle}{\Delta\boldsymbol{k}}\frac{\langle\Phi^{+}_{1,\boldsymbol{k}}\Phi^{-}_{1,-\boldsymbol{k}}\rangle}{\Delta\boldsymbol{k}}\langle f_2\mathrm{e}^{\mathrm{i}\sigma t}\rangle\Delta\boldsymbol{k}, \tag{B 11}$$

with

$$\langle f_2\mathrm{e}^{\mathrm{i}\sigma t}\rangle = \frac{\pi t}{8\sigma\sigma'}\delta\left[\sigma' - (\sigma'' - \boldsymbol{l''}\cdot\boldsymbol{U})\right] + O(1). \tag{B 12}$$

Taking the limit when $\Delta\boldsymbol{k} \to 0$, neglecting bounded terms, and anticipating that only $k'' = k$ gives a non null contribution from the bottom variance yields

$$F^{\Phi}_{2,0}(t,\boldsymbol{k}) = -\int_{\boldsymbol{k''}}\frac{\pi t}{4\sigma''}M^2(\boldsymbol{k},\boldsymbol{k'})F^{B}(\boldsymbol{k}-\boldsymbol{k'})\frac{F^{\Phi}_{0,0}(\boldsymbol{k})}{\sigma'}\delta\left[\sigma' - (\sigma'' - \boldsymbol{l''}\cdot\boldsymbol{U})\right]\mathrm{d}\boldsymbol{k''}. \tag{B 13}$$

Changing the spectral coordinates from $\boldsymbol{k''}$ to (σ'', θ''), one has

$$F^{\Phi}_{2,0}(t,\boldsymbol{k}) = -\int_{\theta''}\int_{\sigma''}\frac{\pi t}{4\sigma''}M^2(\boldsymbol{k},\boldsymbol{k'})F^{B}(\boldsymbol{k}-\boldsymbol{k'})\frac{F^{\Phi}_{0,0}(\boldsymbol{k})}{\sigma'}\frac{k''}{C''_g}\delta\left[\sigma' - (\sigma'' - \boldsymbol{l''}\cdot\boldsymbol{U})\right]\mathrm{d}\sigma''\mathrm{d}\theta''. \tag{B 14}$$

Finally evaluating the integral over σ'' to remove the Dirac distribution and changing again variables from θ'' to θ', we find, including the bounded terms,

$$F^{\Phi}_{2,0}(t,\boldsymbol{k}) = -\frac{\pi t}{4\sigma}\int_{\theta'}M^2(\boldsymbol{k},\boldsymbol{k'})F^{B}(\boldsymbol{k}-\boldsymbol{k'})\frac{F^{\Phi}_{0,0}(\boldsymbol{k})}{\sigma'}\frac{k'}{Cg}\frac{(Cg + \boldsymbol{k}\cdot\boldsymbol{U})}{(Cg' + \boldsymbol{k'}\cdot\boldsymbol{U})}\mathrm{d}\theta' + O(1). \tag{B 15}$$

Appendix C. Resonant wavenumber configuration for $U << C_g$

Under the assumption $U << C_g$, and for a current in the x direction, the resonant conditions

$$\sigma' - \sigma = l_x U, \text{ and} \tag{C 1}$$

yields the following Taylor expansion to first order in $\sigma' - \sigma$,

$$k' - k = (k'_x - k_x)\frac{U}{C_g} + O\left[k\left(\frac{U}{C_g}\right)^2\right]. \tag{C 2}$$

We define, $r = k'$, $r_0 = k$, $r\cos\theta = k'_x$, so that

$$r = r_0 + \frac{U}{C_g}(r_0\cos\theta_0 - r\cos\theta), \tag{C 3}$$

and thus

$$r = \frac{P}{1 + e\cos\theta}. \tag{C 4}$$

This is the parametric equation of an ellipse of semi-major axis a, semi-minor axis b, half the foci distance c, and eccentricity e, with $P = r_0 + U/C_g r_0 \cos\theta_0 = b^2/a$, and $e = U/C_g = c/a$. The interaction between a surface wave with wavenumber $\boldsymbol{k'}$ and a bottom component with wavenumber $\boldsymbol{l}$ excites a surface wave with the sum wavenumber $\boldsymbol{k} = \boldsymbol{k'} + \boldsymbol{l}$. For a fixed $\boldsymbol{k}$ and current U, in the limit of $U << C_g$ the resonant $\boldsymbol{k'}$ and $\boldsymbol{l}$ follow ellipses described by their polar equation (C 4), that reduce to circle for $U = 0$.

REFERENCES

Andrews, D. G. & McIntyre, M. E. 1978 On wave action and its relatives. *J. Fluid Mech.* **89**, 647–664, corrigendum: vol. 95, p. 796.

Ardhuin, F. & Herbers, T. H. C. 2002 Bragg scattering of random surface gravity waves by irregular sea bed topography. *J. Fluid Mech.* **451**, 1–33.

Ardhuin, F. & Herbers, T. H. C. 2005 Numerical and physical diffusion: Can wave prediction models resolve directional spread? *J. Atmos. Ocean Technol.* **22** (7), 883–892.

Ardhuin, F., Herbers, T. H. C., O'Reilly, W. C. & Jessen, P. F. 2003*a* Swell transformation across the continental shelf. part II: validation of a spectral energy balance equation. *J. Phys. Oceanogr.* **33**, 1940–1953.

Ardhuin, F., O'Reilly, W. C., Herbers, T. H. C. & Jessen, P. F. 2003*b* Swell transformation across the continental shelf. part I: Attenuation and directional broadening. *J. Phys. Oceanogr.* **33**, 1921–1939.

Bal, G. & Chou, T. 2002 Capillary-gravity wave transport over spatially random drift. *Wave Motion* **35**, 107–124.

Belibassakis, K. A., Athanassoulis, G. A. & Gerostathis, T. P. 2001 A coupled-mode model for the refraction-diffraction of linear waves over steep three-dimensional bathymetry. *Appl. Ocean Res.* **23**, 319–336.

Berkhoff, J. C. W. 1972 Computation of combined refraction-diffraction. In *Proceedings of the 13th international conference on coastal engineering*, pp. 796–814. ASCE.

Dalrymple, R., Knoght, R. & Lambiase, J. 1978 Bedforms and their hydraulic stability relashionship in a tidal environment, bay of Fundy, Canada. *Nature* **275**, 100104.

Dyer, K. R. & Huntley, D. A. 1999 The origin, classification and modelling of sand banks and ridges. *Continental Shelf Research* **19**, 12851330.

Elfouhaily, T. M. & Guérin, C.-A. 2004 A critical survey of approximate scattering wave theories from random rough surfaces. *Waves in Random Media* **14**, 1–40.

Elter, J. F. & Molyneux, J. E. 1972 The long-distance propagation of shallow water waves over an ocean of random depth. *J. Fluid Mech.* **53**, 1–15.

Fredsøe, J. 1974 Rotational channel flow over small three-dimensional bottom irregularities. *J. Fluid Mech.* **66**, 49–66.

Guazzelli, E., Rey, V. & Belzons, M. 1992 Higher-order Bragg reflection of gravity surface waves by periodic beds. *J. Fluid Mech.* **245**, 301–317.

Hara, T. & Mei, C. C. 1987 Bragg scattering of surface waves by periodic bars: theory and experiment. *J. Fluid Mech.* **178**, 221–241.

Hasselmann, K. 1962 On the non-linear energy transfer in a gravity wave spectrum, part 1: general theory. *J. Fluid Mech.* **12**, 481–501.

Hasselmann, K. 1966 Feynman diagrams and interaction rules of wave-wave scattering processes. *Rev. of Geophys.* **4** (1), 1–32.

Heathershaw, A. D. 1982 Seabed-wave resonance and sand bar growth. *Nature* **296**, 343–345.

Herbers, T. H. C., Hendrickson, E. J. & O'Reilly, W. C. 2000 Propagation of swell across a wide continental shelf. *J. Geophys. Res.* **105** (C8), 19,729–19,737.

Herbers, T. H. C., Orzech, M., Elgar, S. & Guza, R. T. 2003 Shoaling transformation of wave-frequency directional spectra. *J. Geophys. Res.* **108** (C1), 3013, doi:10.1029/2001JC001304.

Hulscher, S. J. M. H. & van den Brink, G. M. 2001 Comparison between predicted and observed sand waves and sand banks in the north sea. *J. Geophys. Res.* **106** (C5), 9327–9338.

Idier, D., Erhold, A. & Garlan, T. 2002 Morphodynamique d'une dune sous-marine du détroit du pas de calais. *Comptes Rendus Géosciences* **334**, 1079–1085.

Kirby, J. T. 1986 A general wave equation for waves over rippled beds. *J. Fluid Mech.* **162**, 171–186.

Kirby, J. T. 1988 Current effects on resonant reflection of surface water waves by sand bars. *J. Fluid Mech.* **186**, 501–520.

Kirby, J. T. & Chen, T.-M. 1989 Surface waves on vertically sheared flows: approximate dispersion relations. *J. Geophys. Res.* **94** (C1), 1013–1027.

Longuet-Higgins, M. S. 1967 On the wave-induced difference in mean sea level between the two sides of a submerged breakwater. *J. Mar. Res.* **25**, 148–153.

Magne, R. 2005 Réflexion des vagues par une topographie sous-marine. PhD thesis, Université de Toulon et du Var.

Magne, R., Ardhuin, F., Rey, V. & Herbers, T. H. C. 2005 Topographical scattering of waves: a spectral approach. *J. of Waterway, Port Coast. Ocean Eng.* **XX**, in press. Available at http://arxiv.org/abs/physics/0504148.

Mei, C. C. 1985 Resonant reflection of surface water waves by periodic sandbars. *J. Fluid Mech.* **152**, 315–335.

Mei, C. C. & Hancock, M. J. 2003 Weakly nonlinear surface waves over a random seabed. *J. Fluid Mech.* **475**, 247–268.

Phillips, O. M. 1977 *The dynamics of the upper ocean*. London: Cambridge University Press, 336 p.

Pihl, J., Mei, C. C. & Hancock, M. 2002 Surface gravity waves over a two-dimensional random seabed. *Physical Review E* **66**, 016611.

Priestley, M. B. 1981 *Spectral analysis and time series*. London: Academic Press, 890 p.

Rayleigh, L. 1896 *The Theory of Sound*, 3rd edn. London: Macmillan.

Rey, V. 1992 Propagation and local behaviour of normally incident gravity waves over varying topography. *Eur. J. Mech. B/Fluids* **11** (2), 213–232.

Rey, V. 1995 A note on the scattering of obliquely incident surface gravity waves by cylindrical obstacles in waters of finite depth. *Eur. J. Mech. B/Fluids* **14** (2), 207–216.

Tolman, H. L. 2002 User manual and system documentation of WAVEWATCH-III version 2.22. *Tech. Rep.* 222. NOAA/NWS/NCEP/MMAB.

Weber, N. 1991 Bottom friction for wind sea and swell in extreme depth-limited situations. *J. Phys. Oceanogr.* **21**, 149–172.

Yu, J. & Mei, C. C. 2000 Do longshore bars shelter the shore? *J. Fluid Mech.* **404**, 251–268.